Geophysical Journal International

Geophys. J. Int. (2014) **198,** 737–759
Advance Access publication 2014 June 3
GJI Geomagnetism, rock magnetism and palaeomagnetism

doi: 10.1093/gji/ggu136

Implications for the lithospheric geometry of the Iapetus suture beneath Ireland based on electrical resistivity models from deep-probing magnetotellurics

C. K. Rao,* Alan G. Jones, Max Moorkamp† and Ute Weckmann§

Dublin Institute for Advanced Studies, 5 Merrion Square, Dublin 2, Ireland. E-mail: alan@cp.dias.ie

Accepted 2014 April 7. Received 2014 April 2; in original form 2013 April 24

SUMMARY

Broad-band and long period magnetotelluric (MT) data were acquired at 39 stations along five NNW-SSE profiles crossing the Iapetus Suture Zone (ISZ) in Ireland. Regional strike analyses indicate that the vast majority of the MT data is consistent with an assumption of a 2-D geoelectric strike direction. Strike is N52°E for the three easternmost profiles and N75°E for the two westernmost profiles; these directions correlate well with the observed predominant geological strike of the study region. 2-D inversions of the galvanic distortion-corrected TE and TM mode data from each profile are shown and discussed. As mapped geological variations between the neighbouring profiles suggest a heterogeneous subsurface, it is important to verify the robustness of the presence and geometries of prominent conductivity anomalies by employing 3-D forward and inverse modelling. A high conductivity layer (resistivity of 1–10 Ωm), found at middle to lower crustal depths and presumed to be indicative of metamorphosed graphitic sediments rich in sulphides deposited during the convergence of the Laurentian and Avalonian continents, essentially constitutes the electrical signature of the ISZ. Shallow conductors observed are probably due to black shales that were widely deposited within the sedimentary accretionary wedge during Ordovician time. We interpret the moderately low resistivity at shallow depths from west to east across Ireland as indicative of an increase in maturity of the black shales in the easterly direction. From our conductivity models the southern extent of the ISZ is inferred to lie between the Navan Silvermines Fault and the Navan Tipperary Line, and shows clear resistivity contrast along all the profiles at the southern MT stations. The change in resistivity deduced from the 2-D models is spatially related to the composition of Lower Palaeozoic Ordovician, Silurian, Devonian and Carboniferous rocks. At upper mantle depths of about 60 km, a high conductivity block below the central MT stations is found to lie within the accretionary wedge of the Iapetus suture, and the location of the conductive anomaly corroborates reasonably well with the inferred spreading head of the putative Iceland plume-related magmatic intrusion. The low resistivity upper crust beneath the ISZ is indeed rich in Ordovician rocks with black shale content in the eastern as well as the central part; the western part is largely underlain by a highly resistive block of volcanic and metamorphosed rocks forming crystalline basement.

Key words: Electrical properties; Magnetotellurics; Composition of the continental crust; Continental margins: convergent; Crustal structure; Europe.

INTRODUCTION

The collision of the Laurentian and Avalonian continents during early Devonian times (400 Ma) closed the Iapetus Ocean and resulted in a major linear tectonic boundary in the UK, Ireland, easternmost Canada and easternmost USA known as the Iapetus Suture Zone (ISZ). The length extent of the suture between Avalonia and Laurentia is approximately 1270 km (Phillips *et al.* 1976). The ISZ

* Now at: Indian Institute of Geomagnetism, Navi Mumbai, 410218, India
† Now at: Department of Geology, University of Leicester, Leicester LE1 7RH, UK
§ Now at: Helmholtz Centre Potsdam – German Research Centre for Geosciences, Telegrafenberg, D-14473 Potsdam, Germany

is defined as the zone separating continental crustal blocks on opposing margins of this early Paleozoic Ocean, the Iapetus Ocean, and is recognized as one of the earliest geological indicators of the 'Wilson-cycle' of ocean opening and closing (Wilson 1966). The evidence for the trace of ISZ in Britain and Ireland has been reviewed by Todd *et al.* (1991) using five different types of data sets; faunal, tectono-stratigraphic, structural, geophysical and isotopic.

At surface, the ISZ is well expressed in the Southern Uplands of Scotland and Newfoundland (Canada), and can be followed into the Appalachians of North America [see Ogawa *et al.* 1996; Wannamaker *et al.* 1996 for magnetotelluric (MT) studies in the Appalachians], but in Ireland its trace is mostly obscured by lack of surface expression. Consequently, the location of the ISZ relies upon scant geological field evidence together with anomalies and structures inferred from geophysical experiments. In the past three decades the Iapetus suture and its tectonics have been widely studied in Britain and Ireland by several workers using many geological and geophysical methods (see, for example; Phillips *et al.* 1976; Max *et al.* 1983; McKerrow & Cocks 1986; Denny 2000; Landes *et al.* 2003; Tauber *et al.* 2003; Polat *et al.* 2012).

In terms of electromagnetic imaging of the ISZ, Jain (1964) was the first to conduct an electromagnetic study of the ISZ, although he was not aware of the tectonic context at that time. He discovered a geomagnetic anomaly in the Southern Uplands of Scotland and named it the 'Eskdalemuir anomaly' (after the geomagnetic observatory in the town of Eskdalemuir from which he used the data). Subsequently Edwards *et al.* (1971), then Jones & Hutton (1977, 1979a,b) and Hutton & Jones (1980) and later Parr & Hutton (1993) identified different conductive blocks in this region, which provided a basis to define the geometry of the suture zone. More recent MT studies corroborate earlier results (Tauber *et al.* 2003; McKay & Whaler 2006).

In the Irish segment of the ISZ, the first MT studies were carried out in the 1990s and early 2000s. The first study (Whelan *et al.* 1990) discovered an anomalous middle to lower crustal conductor that was interpreted as the complex manifestation of the Iapetus Suture, based on 1-D inversions of the MT data. Brown & Whelan (1995) further modelled the same data using 2-D inversion. They identified two upper crustal conductors and interpreted as them as weakly metamorphosed black shales in sedimentary basins. The VARiscan NETwork (VARNET) MT studies of Brown *et al.* (2003) in south-west Ireland identified a near-surface conductive zone associated with the east–west trending Killarney-Mallow Fault Zone (KMFZ, Fig. 1). These prior MT studies in Ireland investigated only structures shallower than 7 km, based on the available short period data and equipment, processing and interpretation techniques used during the surveys.

With the availability of state-of-the-art MT equipment covering a wide frequency range (proxy for depth), together with modern and improved methods and techniques for processing, analysis, modelling and inversion, we conducted MT measurements across the ISZ during the years 2004–2006. Using the broad-band MT (BBMT) data from one NW–SE profile located in eastern Ireland, Rao *et al.* (2007) identified a U-shaped highly conductive zone (vertically integrated conductance of 2000–7000 S) in the central part of eastern Ireland (from MT stations 105 to 110; Fig. 1) that was interpreted in terms of metamorphosed graphitic sediments within the ISZ.

This paper comprehensively describes all of the MT investigations followed by in-depth interpretation of the results obtained from the four other NW–SE profiles, together with the inclusion of longer period, mantle penetrating data along the main profile (the eastern NW–SE Profile). 2-D and 3-D modelling and inversion are used to determine the robustness of imaged features.

GEOLOGICAL SETTING

The geology of Ireland comprises Paleozoic and, to a lesser extent, Precambrian rocks covering the entire region (Daly 2001) that were affected by Caledonian Orogeny events. These events are limited to the earlier arc-continent collision Grampian event (475–460 Ma, Soper *et al.* 1999) and a Caledonian event, predominantly the closure of the Iapetus Ocean that joined the Laurentian Plate in NW Ireland with the Avalonian Plate in SE Ireland (Dewey 1969; Ryan & Devy 1991). Grampian events affected only the Midland Valley terrane and the ISZ. Although the ISZ was formed in the late Silurian to early Devonian, it may well have been structurally modified by later Acadian and Variscan events (Woodcock *et al.* 2007). During Caledonian times, the bulk of the Irish crust was assembled from a series of independent terranes into linear NE-SW zones (Murphy *et al.* 1991). Among them, from north to south, the Grampian, Midland Valley, Central and Leinster terranes constituted major terranes; they are shown in Fig. 1 together with the locations of the MT sites.

The Grampian terrane in northwest Ireland is bounded by the Highland Boundary Fault (HBF)/Fair Head Clew Bay Line (FCL) to the south. The terrane south of the HBF/FCL comprises the Midland Valley terrane containing Cambrian to Carboniferous rock units (Murphy *et al.* 1991; Long 2003). Further south of this lies the Central terrane, where much of our present work is focussed. The major faults in this terrane include the northern-bounding Southern Uplands Fault (SUF; Max *et al.* 1983), the Orlock Bridge Fault (OBF; Anderson & Oliver 1986), the Navan Silvermines Fault (NSF), and the southern-bounding Navan Tipperary Lineament (NTL; Archer 1981; Max *et al.* 1983).

PREVIOUS GEOPHYSICAL STUDIES

A number of geophysical studies have been carried out across the ISZ in Britain and Ireland since the 1970s to define its presence, geometry and location. Seismic experiments conducted across terranes of the ISZ in the UK were reviewed in Chadwick & Pharaoh (1998), and for Ireland by Landes *et al.* (2005). All of the UK studies identified a northward-dipping zone of reflectors (25°– 40°) at a depth of 15–30 km in the vicinity of the ISZ.

Pioneering geomagnetic and electromagnetic studies by Edwards *et al.* (1971), Hutton *et al.* (1977), Jones & Hutton (1979a,b), and Hutton & Jones (1980) revealed the presence of a major conductivity anomaly across southern Scotland within generally more resistive rocks in the lower crust. Subsequent MT studies of the ISZ in Scotland were conducted by Sule & Hutton (1986), Sule *et al.* (1993), Harinarayana *et al.* (1993) and Livelybrooks *et al.* (1993). Based on 2-D modelling of the available MT data, Livelybrooks *et al.* (1993) inferred a mid-crustal conductor at approximately 10 km depth characterizing the ISZ. More recently Tauber *et al.* (2003), employing a high resolution MT survey across the Southern Uplands of Scotland, imaged conductive blocks that appeared to be laterally terminated by known faults.

The cause of the conductivity anomaly associated with the ISZ has been widely speculated, even from the earliest work where three explanations were proffered: (i) an extinct magma chamber containing iron-rich olivine, (ii) high water content in deformed marine sediments or (iii) graphitic schists (Edwards *et al.* 1971). Banks

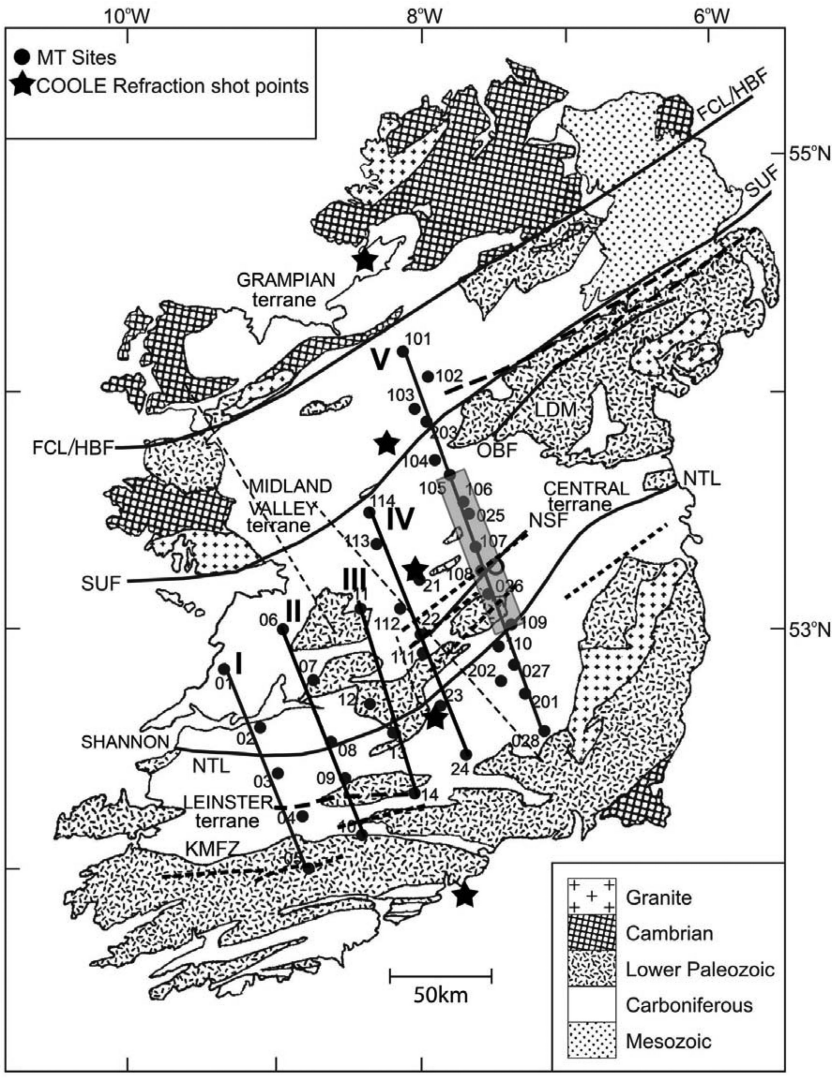

Figure 1. Simplified geological map of Ireland with 39 MT sites along five profiles (I–V) and major faults: FCL/HBL, Fair Head Clew Bay Lineament/Highland Boundary Fault; SUF, Southern Uplands Fault; OBF, Orlock Bridge Fault; NSF, Navan Silvermines Fault; NTL, Navan Tipperary Lineament, KMFZ, Killarney Mallow Fault Zone. LDM, Longford-Down Massif. The shaded region represents the U-shaped conductor identified by Rao *et al.* (2007). Thick and thin dashed lines represent NE–SW, ENW–WSE and NW–SE lineaments deduced from gravity studies (Readman *et al.* 1997).

et al. (1996) considered many possible candidates, and concluded that the most likely explanation is mineralogy rather than fluids, in this case the presence of graphite. Metallic mineralization or graphite was also the conclusion of Tauber *et al.* (2003) from their focussed study in which the boundaries of the anomaly were related to strike-slip faults.

The continuation of the ISZ into Ireland, and its structural properties along this section of the suture, have been investigated in a number of geophysical experiments conducted over the last three decades, primarily by passive and active source seismology studies (Max *et al.* 1983; Lowe & Jacob 1989; Klemperer *et al.* 1991; Brown & Whelan 1995; Readman *et al.* 1997; Denny 2000; Brown *et al.* 2003; Landes *et al.* 2005; Do *et al.* 2006; Landes *et al.* 2007; Rao *et al.* 2007; Hauser *et al.* 2008; Wawerzinek *et al.* 2008; O'Donnell *et al.* 2011; Polat *et al.* 2012). Gravity studies in Ireland (O'Reilly *et al.* 1996; Readman *et al.* 1997) identified three major trends in gravity anomalies: the NE–SW Caledonian trending lineaments, subsidiary NNE-SSW trending lineaments and weaker NW–SE trending lineaments.

The crustal structure in the vicinity of Iapetus Suture in Ireland was studied by seismic refraction experiments, beginning with Irish Caledonian Suture Seismic Project in the early-1980s (Jacob *et al.* 1985), followed by COOLE (Caledonian onshore-offshore lithospheric experiment; Lowe & Jacob 1989), VARNET-96 (VARiscan Network; Landes *et al.* 2000, 2003) and Leinster Granite Seismics (Hodgson 2001). All of these were later reviewed in detail by Landes *et al.* (2005) and the presented Moho topography was derived from 2-D velocity models along seismic profiles conducted across Ireland. Those authors showed a Moho depth for Ireland varying between 28.5 and 32 km. Receiver function (RF) studies (Landes *et al.* 2006) showed minor structural changes across the ISZ in the crust-mantle boundary, and these were interpreted in terms of post-Caledonian tectonic movements. Joint analysis of shear and compressional wide angle seismic data from south-western Ireland (Hauser *et al.* 2008) inferred that the Irish crust is unusually felsic in bulk composition based on the mean value (∼0.247) of Poisson's ratio (σ) for the Irish crust as compared to the mean global average value of σ (∼0.265). These studies also revealed that the upper crust

is chemically differentiated into a silica rich region (∼75 per cent ∼20 km thick) whereas the lower crust (∼10 km thick) is silica-rich but is comparatively depleted (∼64 per cent).

Non-linear tomography studies in Ireland (Wawerzinek *et al.* 2008) indicated a negative traveltime anomaly (faster *P*-wave velocity) in the western part, and a positive anomaly (slower *P*-wave velocity) in the eastern part of Ireland. This east–west disparity was observed for all depths, and is particularly pronounced in the upper mantle (31–60 km) with over 2 per cent *P*-wave velocity perturbation (figs 6 and 7 of Wawerzinek *et al.* 2008). Joint inversion of teleseismic and gravity data from Ireland (O'Donnell *et al.* 2011) imaged anomalies at lithospheric depths greater than 50 km owing to compositional contrasts, either due to terrane accretion associated with Iapetus Ocean closure, frozen Iceland plume magmatic intrusions or a combination of both. Most recently, a surface wave dispersion study from the teleseismic Irish Seismological Lithospheric Experiment (ISLE) and Irish Seismic Upper Mantle Experiment (ISUME) experiments showed strong crustal anisotropy for the whole of the island of Ireland, with the fast axis direction approximately NE–SW (Polat *et al.* 2012), consistent with the approximate direction of the ISZ. The Rayleigh wave phase velocity anomaly maps at various periods from the tomographic inversion modelling do not show NE–SW trends though, but rather exhibit strong east–west differences, up to 4 per cent, particularly for those periods where the Fréchet derivatives are sensitive to the upper crust (10 s) and those sensitive to the lower crust and upper mantle (25 s, 30 s; fig. 3 of Polat *et al.* 2012), consistent with the findings of Wawerzinek *et al.* (2008).

The interpretation of seismic data across Ireland (Jacob *et al.* 1985; Lowe & Jacob 1989) inferred the ISZ is characterized by thickening of middle crustal layer and lateral changes in crustal velocities are interpreted as crustal deformation from orogenic collision different crustal units. Consequent studies (VARNET-96 Landes *et al.* 2000) showed an anomaly in *P*-wave residual across ISZ, and the model is unable to explain the magnitude of delay times. ISLE (Landes *et al.* 2004) was designed to test the idea that the traveltime anomaly is due to seismic anisotropy within the upper mantle below the crustal manifestation of the ISZ.

Among the MT studies conducted across the ISZ in Ireland (Brown & Whelan 1995; Denny 2000; Brown *et al.* 2003; Rao *et al.* 2007), short period MT measurements (Brown & Whelan 1995) revealed two major upper crustal conductors, each associated with terrane boundaries that are interpreted to have developed probably during Caledonian orogeny. One of these conductors is inferred to dip south-eastwards with an angle of 8° from a depth of 5.5 to 10 km, and was interpreted to be composed of weakly metamorphosed black shales in a sedimentary basin that underthrusts the Laurentian and Avalonian continents. While the earlier MT studies (Brown & Whelan 1995; Denny 2000; Brown *et al.* 2003; Rao *et al.* 2007) focussed only on shallow structures to a depth of few kilometres, this study aims at augmenting the seismic ISLE experiment and to image the ISZ and its geometry at much larger depths covering the lithosphere. These new results will provide a link between the UK segment of the ISZ in the east and the Canadian segment in the west.

MT DATA ACQUISITION, PROCESSING AND ANALYSIS

We acquired MT data in three different phases between 2004 February and 2006 January at a total of 39 locations along five NW–SE profiles (Fig. 1), numbered I to V, as part of the ISLE-MT (Irish magnetotelluric lithosphere experiment) project. During the first phase, data were collected at 22 stations at the same locations as the ISLE seismic sites (Landes *et al.* 2004, 2006) with two different sets of equipment: broad-band (period range 0.003–3000 s) Phoenix Geophysics MTU-V5A systems and long period (LMT, period range of 20 s to over 10 000 s) LiMS systems (Anderson *et al.* 1988; Narod & Bennest 1990) that were provided by the Geological Survey of Canada. These 22 sites are labelled 01–14 and 21–28 in Fig. 1. The BBMT time-series were recorded for 2–3 nights, and the LMT time-series were recorded for 6–8 weeks at each location.

In the second phase, 14 additional BBMT stations were deployed between the existing BBMT + LMT sites and extending the easternmost site to the north to improve spatial coverage; they are labelled 101 to 114 (Fig. 1). In addition, long period data were recorded afterwards for 3–4 weeks at stations 101 to 110 using GEOMAGNET systems from the Geophysical Instrument Pool Potsdam (GIPP). During the third, smaller, phase, three more BBMT stations (201–203; Fig. 1) were included in the main profile to enhance resolution of detected structures. At all locations, electric field variations in the north–south and east–west orthogonal directions were measured using non-polarizable Ag/AgCl or Pb/PbCl electrodes in an X-configuration with typically 50 m arms. The magnetic field sensors used for BBMT acquisition were Phoenix MTC-50 induction coil magnetometers, and for the LMT systems were ring-core fluxgate magnetometers.

The notion of having the MT instruments as close as possible to the ISLE seismic sites during the first phase was to facilitate development and application of a new joint inversion approach for teleseismic and MT data (Moorkamp *et al.* 2007, 2010; Roux *et al.* 2011), but this imposed severe constraints on possible MT site locations. All of the ISLE seismic sites, which were established prior to the initiation of the ISLE-MT project, were installed on farm lands that were surrounded by electric cow fences. Strong signal contamination due to these electric fences rendered the MT data at short periods (<1 s) highly distorted and unusable, even after attempting to remove the effects using several robust, remote-reference codes (methods 6, 7 and 8 in Jones *et al.* 1989) as well as bounded influence methods (Chave & Thompson 2004). Fig. 2 illustrates an example of contaminated (Fig. 2a) and uncontaminated (Fig. 2b) time-series, and their corresponding apparent resistivity and phase estimates. To address the contamination problems, the short period data (<1 s) at most of the sites acquired in first phase (01–28) were deleted from further processing, analysis and modelling. Consequently, we have lower resolution of upper crustal structures and associated features at these sites than at the others recorded in phases II and III.

The BBMT and LiMS LMT time-series data were processed using robust remote reference techniques (Jones & Jödicke 1984; Jones *et al.* 1989) based on a robust approach proposed independently called Least Trimmed Squares (Rousseeuw 1984; Rousseeuw & Leroy 1987). The GIPP GEOMAGNET LMT data were processed following Ritter *et al.* (1998) and Weckmann *et al.* (2005). Where LMT data were available, either from LiMS or GEOMAGNET systems, their responses were merged with the corresponding BBMT response estimates. Satisfactorily, estimates at overlapping periods from the BBMT and LMT systems were within each other's error estimates, not only for the off-diagonal terms (XY and YX), but importantly also for the diagonal terms (XX and YY) of the MT impedance tensor.

The responses were then subjected to galvanic distortion identification and correction with a tensor decomposition approach using

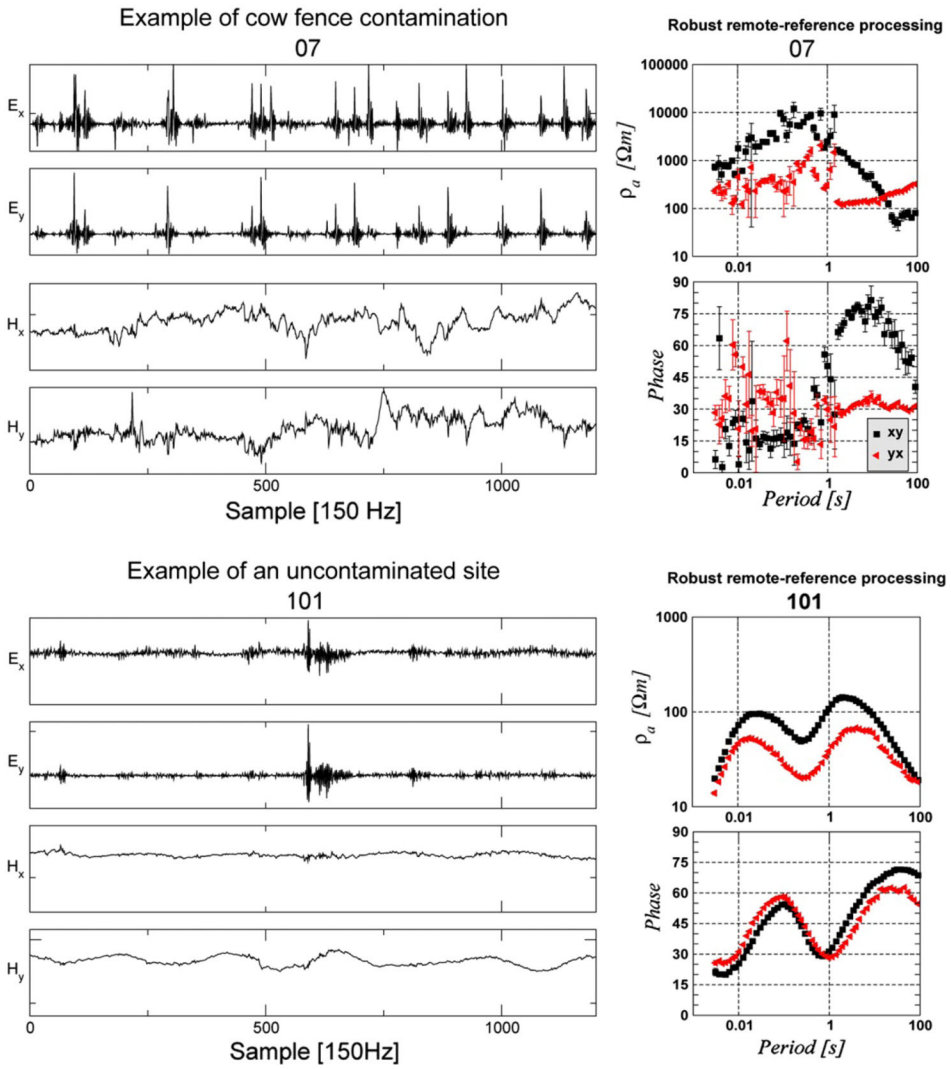

Figure 2. Example of (a) Electric cow fence contaminated time-series and its corresponding resistivity and phase curve. (b) Uncontaminated time-series and its corresponding resistivity and phase curve.

the multisite, multifrequency analysis code of McNeice & Jones (2001) on subsets of sites. The superiority of applying a model of galvanic distortion within a statistical reference frame over other methods that simply re-arrange and manipulate the MT impedance tensor estimates is outlined in detail in Jones (2012). As a result of strike and distortion analyses, we derived the estimates of the regional MT impedances for the two different 2-D MT modes, TE and TM, representing current systems parallel (TE) and perpendicular (TM) to the subsurface geoelectric strike direction. Fig. 3 shows the single-site regional geo-electric strike directions for four different decade-wide period bands at all sites. The error (normalized rms misfit) in the distortion models was less than 2 at most of the sites at all periods, except for some stations (13, 23, 26, 104 and 109). At sites 13, 23 and 26, the whole frequency range (20–10 000 s) did not show an acceptable fit, whereas at stations 104 and 109 the data at periods of 20 s and above are affected (rms error greater than 2). At sites 13, 23, 26 and 109, the distortion appears to be mainly due to severe current channelling as these stations are located close to the edges of geological bodies (Fig. 1). At station 104 the TE mode phases are out of quadrant. The data at station 104 exhibit a different rotational angle to the regional strike direction of N52°E; that station lies close to the OBF (Fig. 1) and is probably affected by it. In the regional strike direction its phases are out of quadrant. As we will show below, the model retrieved using 3-D inversion suggests a nearby strong conductivity contrast that is likely the cause this phase behaviour.

Fig. 4 shows the rms error misfit for the strike analysis averaged over each period band (1–10, 10–100, 100–1000, 1000–10 000 s) for each of the profiles, where all sites on each of the profiles have been modelled together. Multisite, multifrequency analyses of the two western most profiles (I and II; Fig. 1) suggest that the regional electric strike is best-defined in the direction of N75°E, and the three eastern profiles (III, IV and V) yield a best fitting strike direction of N52°E. In both cases, the strike directions are consistent with major gravity trends of ENE–WSW in western Ireland and NE–SW in eastern Ireland.

The tensor decomposed regional impedances of the TE and TM mode data for all the five profiles are shown as apparent resistivity and phase pseudo-sections in Figs. 5(a)–(e). The most striking features of the phase pseudo-sections in both the TE and TM modes of profiles IV and V are the high phase values observed at periods of 10–100 s over much of the two profiles; these high phases at those periods indicate enhanced electrical conductivity at depths <20 km. The TM mode data show a change in phase at 1000 s at stations

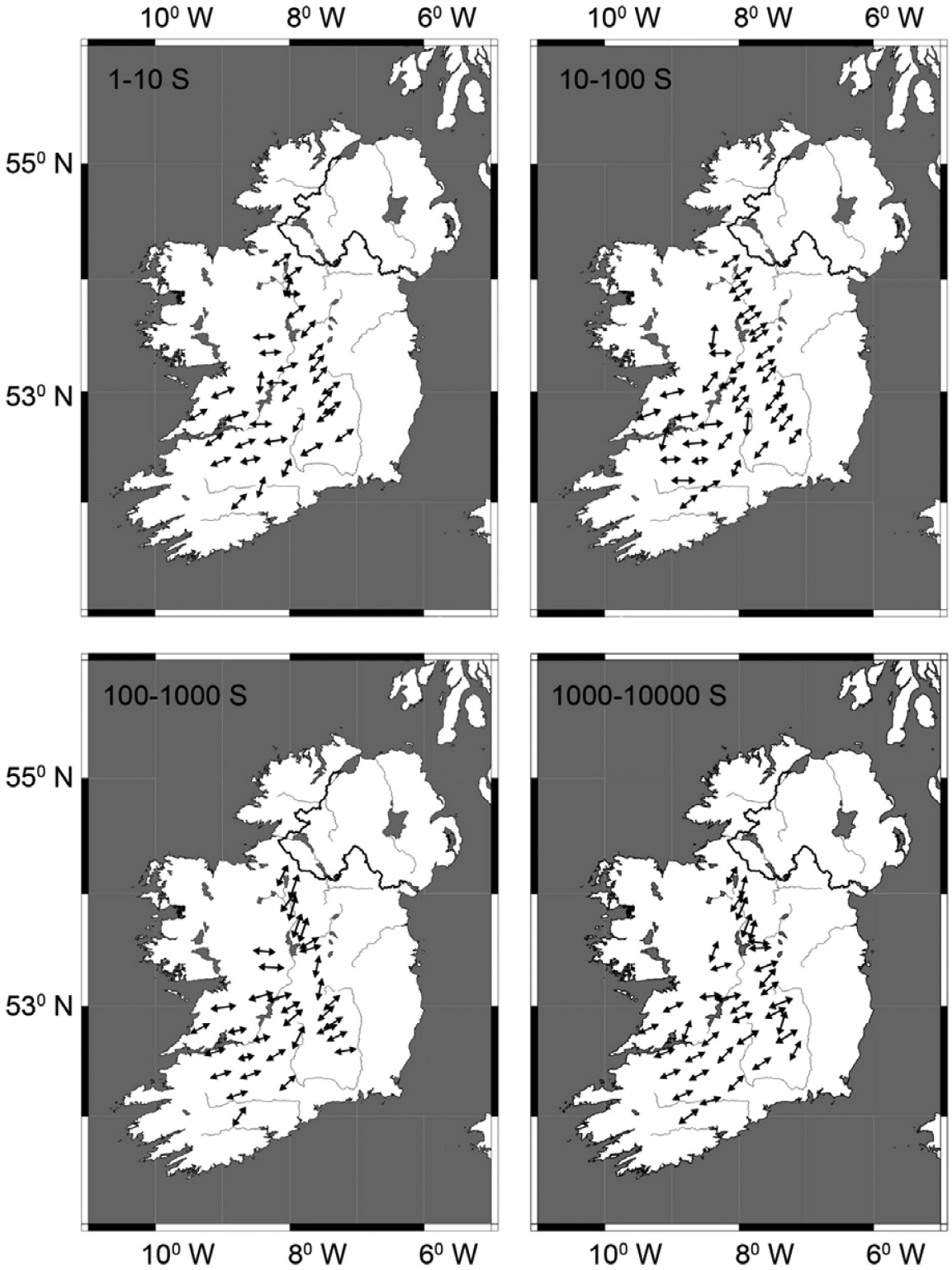

Figure 3. Regional geo-electric strike at 1–10, 10–100, 100–1000 and 1000–10 000 s obtained by using the multisite, multifrequency analysis code (McNeice & Jones 2001).

105–25 on profile V, and at stations 111 to 112 on profile IV. Such a change in phase is not seen at other stations, presumably owing to considerable attenuation of longer periods at those stations. Phase pseudo-sections below stations 101–203 (Fig. 5d) at periods 10 to 1000 s show high phase $>45^\circ$ (conductive), in both TE and TM modes. The density of the stations and the high quality of the data on profiles IV and V (Figs 5d and e) give us confidence that the observed abrupt lateral changes in phases on these profiles are real and are not an artefact of spatial under sampling or poor data quality. All phase pseudo-sections (Figs 5a–e) exhibit evidence that the conductivity of the structures increases (phase increases from $<45^\circ$ to $>45^\circ$) from west to east in the study region.

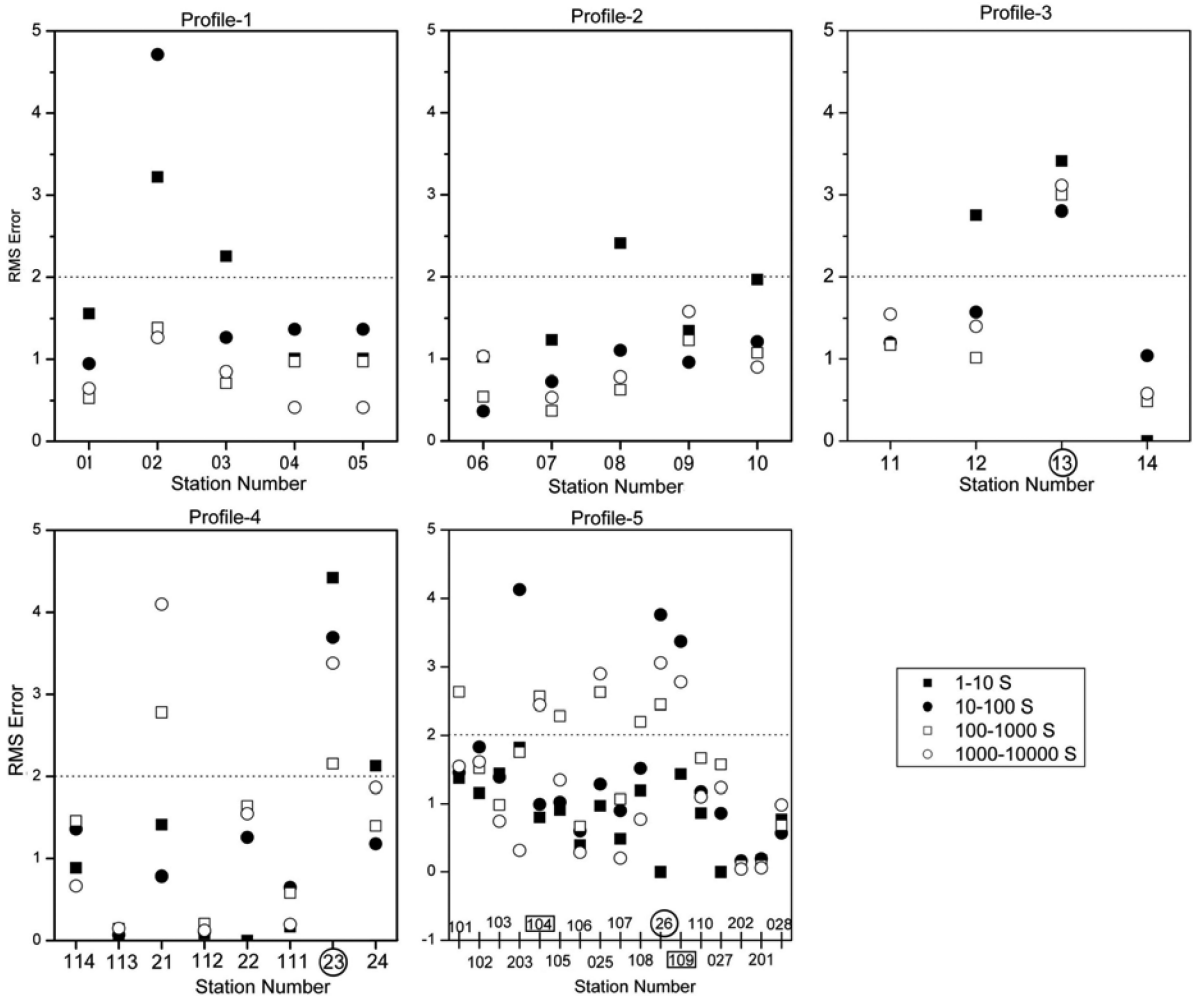

Figure 4. The rms misfit of regional strike for all five profiles period averaged over period bands 1–10, 10–100, 100–1000 and 1000–10 000 s and rms <2 indicate the valid strike angle obtained using the multisite, multifrequency analysis code (McNeice & Jones 2001). The results from the stations whose numbers are marked with a circle do not fit the strike angle at all frequencies, and whereas stations marked with square boxes the strike angle does not fit above 20 s.

2-D INVERSION AND RESULTS

The MT data (TE, TM modes and vertical magnetic Hz tipper) from all five profiles were inverted using the 2-D RLM2-DI algorithm (Rodi & Mackie 2001), as implemented within the WinGLink package of Geosystem Srl. (now Schlumberger/Western Geco). The TE data at two stations (05 on profile I, 104 on profile V) and the TM data at one station (07 on profile I) were removed prior to inversion since these data exhibit severe distortion effects that could not be corrected by distortion decomposition analysis and are likely are due to 3-D effects and different rotation angles. A homogeneous half-space, with a resistivity of 100 Ωm, was used as a starting model for all inversions. By performing a number of inversions with different regularization parameters τ in an L-curve manner (Hansen 1992), we identified the optimum trade-off between data misfit and model roughness (Fig. 6) for profile V and used this optimal value for all other profiles. The error floors for the TE and TM mode apparent resistivities and phases for all the sites were set to 10 and 5 per cent (equivalent to 1.5 degree) and 7 and 5 per cent, respectively. We selected a slightly higher error floor (10 per cent) for the TE mode apparent resistivities as the TE mode data are more sensitive to residual 3-D effects (e.g. Jones 1983; Wannamaker *et al.* 1984; Ledo *et al.* 2002; Ledo 2005). After 50–100 iterations, magnetic tipper data were included in the inversion. We observed that too early introduction of tipper results in the inversion gave too much weight to those data at the cost of underfitting the MT data. This is because tipper data are only responsive to anomalies in conductivity, especially strong conductivity contrasts, and are insensitive to the overall conductivity background. The absolute error for the magnetic field transfer function was selected as 0.015 in the inversion. After a small number of iterations (10–20), static shifts were switched on at some sites and treated as unknowns within the inversion procedure, following the standard approach of deGroot-Hedlin (1991). We selected those sites for static shift correction that show a generally parallel trend between the TE mode calculated and observed curves, especially at high frequencies.

Induction arrows (Parkinson convention; real arrows reversed to point towards conducting anomalies) at some representative periods are shown in Fig. 7. Induction arrows are typically perpendicular to a lateral conductivity contrast and their magnitude is indicative of the relative conductivity changes. In the study area between the periods 10–100 s most of the arrows are generally small except at stations close to the Atlantic Ocean. There is no clear trend in these vectors and some of them point parallel and perpendicular to strike direction. At a period of 1000 s the induction arrows at the north-western stations of profile V are pointing towards the

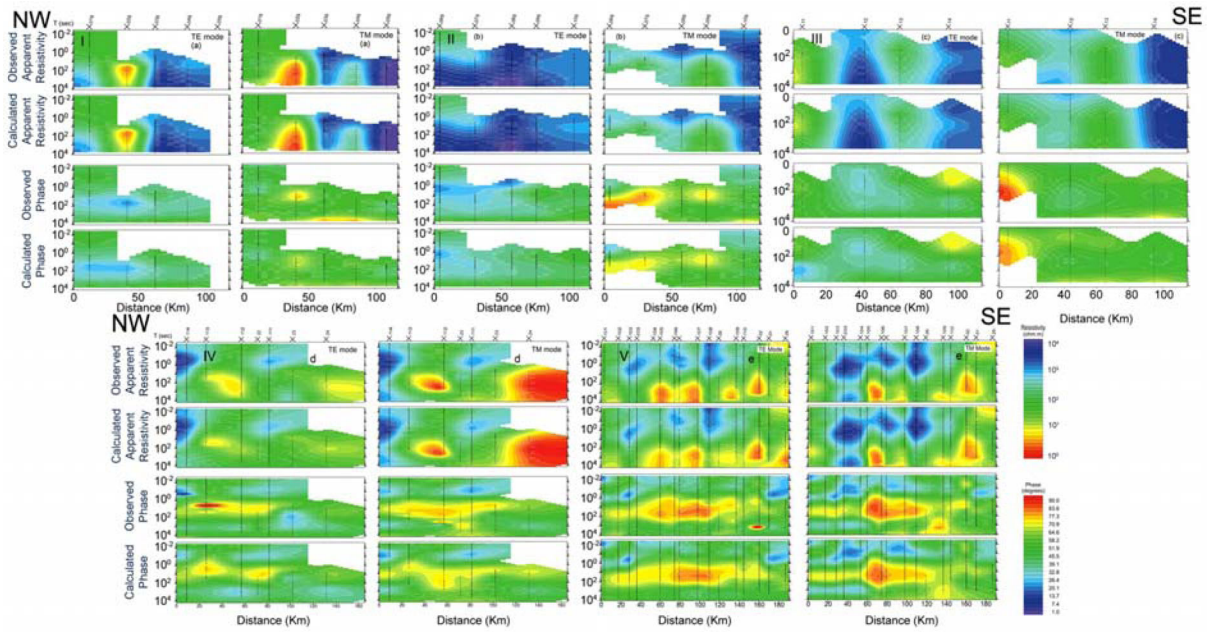

Figure 5. (a)–(e) Pseudo-sections of TE & TM modes apparent resistivity and phase of the observed and the modelled data with data points shown on the observed data contours of profile I through profile V, respectively.

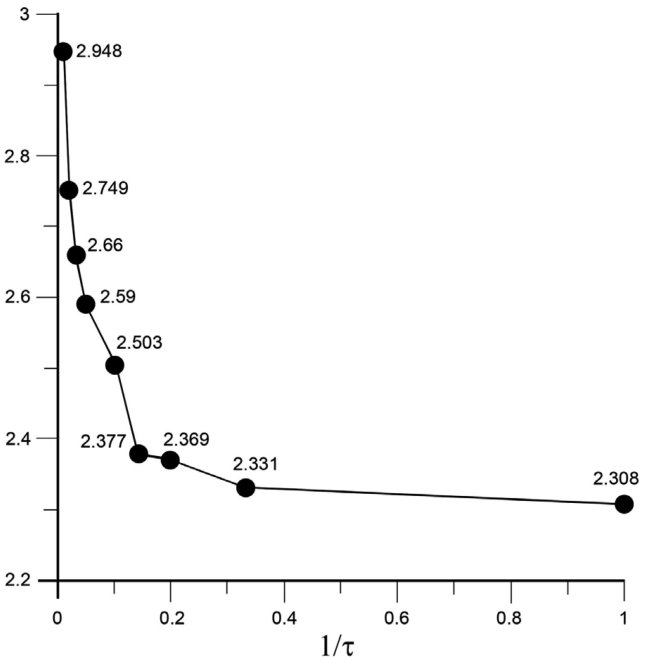

Figure 6. Roughness against model fit trade-off curve (L-curve) obtained for different smoothness regularization parameters (τ) versus rms values for 2-D inversion models. τ is plotted along the abscissa by its inverse, as high τ values invoke a high weighting for the smoothing, and hence a degree of smoothing, and low τ values a low degree of smoothing. A τ value of 7 ($1/\tau$ of 0.14) represents the 'knee' in the L-curve with an rms of 2.377.

west. Since the magnitudes of these arrows are small (<0.3), they likely are indicating conductivity contrasts in the lower crust. At a period of 5000 s all arrows are pointing towards the west due to the strong conductivity contrast between the Atlantic Ocean and the land.

After many hundreds of iterations per profile and per run, best-fitting models were selected with normalized rms values shown for each individual profile in Fig. 8. The final resistivity models for all the profiles and interpolated depth slices are shown in Figs 8 and 9, respectively, and the model responses are presented in Figs 5(a)–(e) (2nd and 4th row in each column). In Fig. 8 we label the main features of the geo-electric models, from east to west. These are as follows:

(1) Prominent conductors (marked C1-C7) exist at upper to lower crustal depths. The composite conductor has an apparent NW and SE dip at the ends of the profiles from upper to lower crustal depths below profiles III, IV and V, whereas it is defined only in the upper and middle crust along the profiles I and II.

(2) A highly anomalous conductor (marked UMC) is present in the upper mantle at a depth of about 60 km south of the surface trace of the OBF below stations 106–107 on profile V.

(3) The middle and lower crust below profiles I, II and III generally exhibit high resistivities of several thousand Ωm.

(4) We observe a change from high resistivity in the western part to low resistivity in the eastern part of Ireland (Fig. 9) at all crustal levels and into the lithospheric mantle.

(5) At very shallow depths (∼2 km); a resistive body (feature R1) is delineated below the northernmost stations of the profile V.

All first-order features listed above are robust in the 2-D models, in that they are found with varying subsets of the data and varying inversion parameters and varying starting models.

3-D FORWARD MODELLING

We undertook 3-D forward modelling to verify the robustness of the main features obtained using 2-D inversion. In comparison with 2-D, 3-D forward modelling is time-consuming because of the fine grid requirements for resolving conductivity contrasts. We used the 3-D forward modelling code (MT3-DFLOD) of Mackie & Booker (1999), as implemented in WinGLink, for modelling all five profiles and the island of Ireland. Due to memory limitations, a mesh size

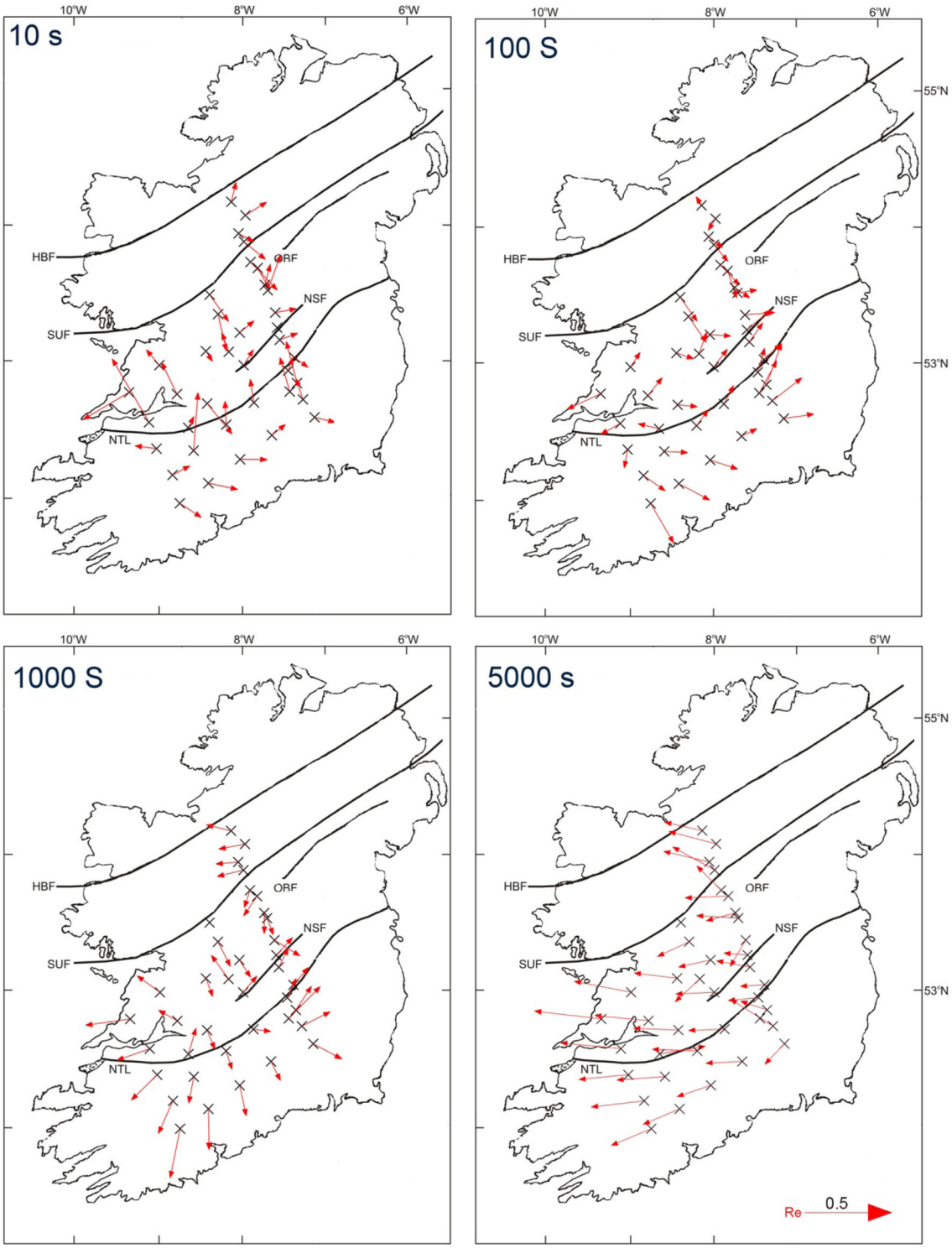

Figure 7. Real induction arrows (Parkinson convention) at 10, 100, 1000 and 5000 s with known major faults: HBL, Highland Boundary Fault; SUF, Southern Uplands Fault; OBF, Orlock Bridge Fault; NSF, Navan Silvermines Fault; NTL, Navan Tipperary Lineament.

of 44 × 59 × 39 cells was used for the grid. To achieve convergence we selected a cell size of 200 m in the vertical (Z) direction closest to the surface and increased it progressively with depth. The ocean was represented by a layer of 150 km in width and 200 m in thickness close to land with gradual increase in thickness of the layer to 2.5 km at distance based on the bathymetry of the region. The depth sections from the 2-D models obtained along the five profiles were used for building the initial forward 3-D conductivity model. A uniform layer of low resistivity (10 Ωm) was selected below the 3-D model to represent the asthenosphere. Forward solutions were derived in seven decade period bands, six discrete periods per decade, and were compared to original (un-decomposed) MT impedance responses. After 115 trial-and-error forward models, the synthetic responses reproduce the main features of the observed data at all

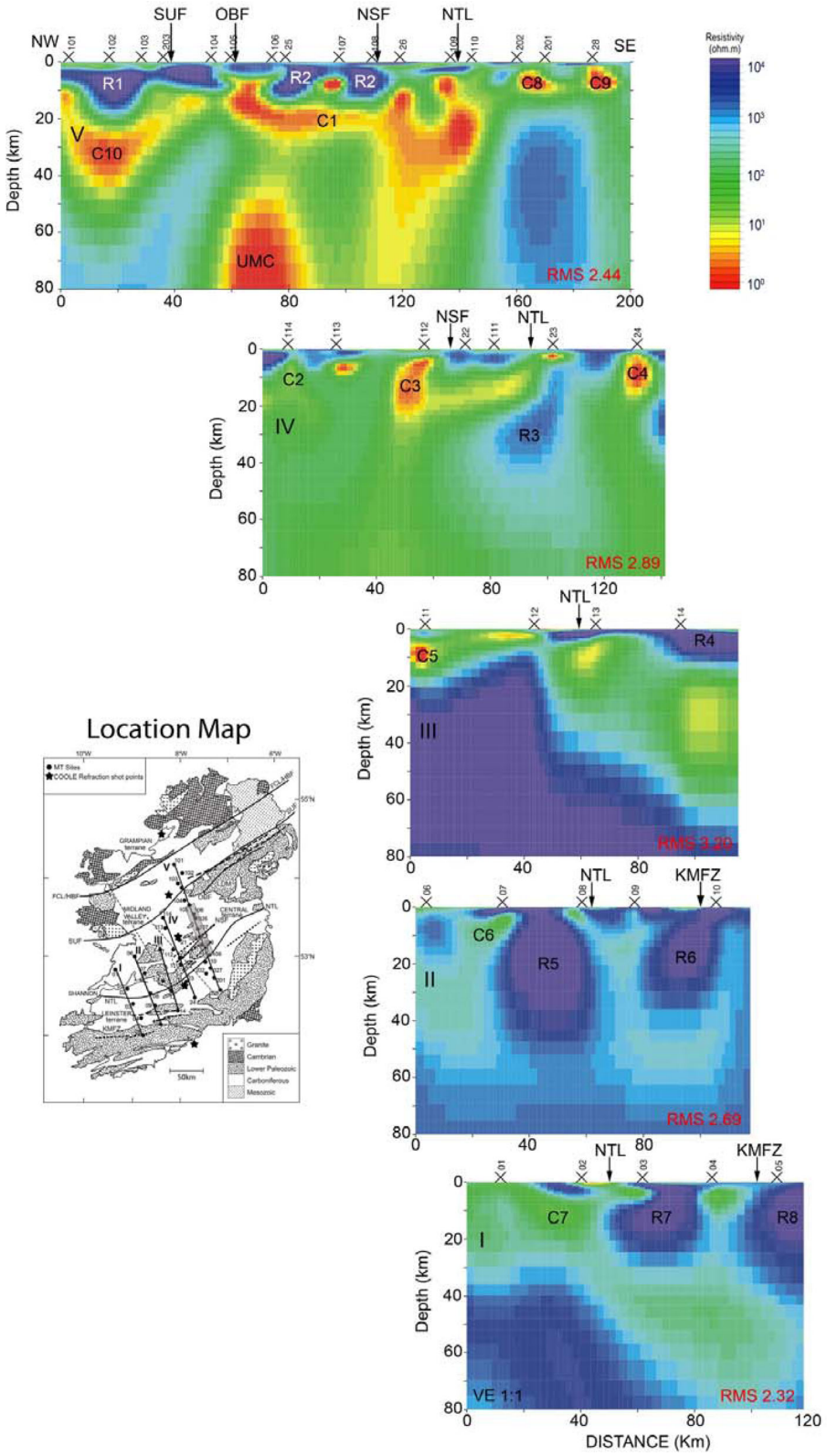

Figure 8. Geo-electric sections across the Iapetus Suture Zone along all five profiles in Ireland obtained from 2-D inversion of MT (TE, TM and HZ) data with inset of MT profiles. Top to bottom; Geoelectric section of profile V through Profile I; SUF, Southern Uplands Fault; OBF, Orlock Bridge Fault; NSF, Navan Silvermines Fault; NTL, Navan Tipperary Lineament; KMFZ, Killarney Mallow Fault Zone.

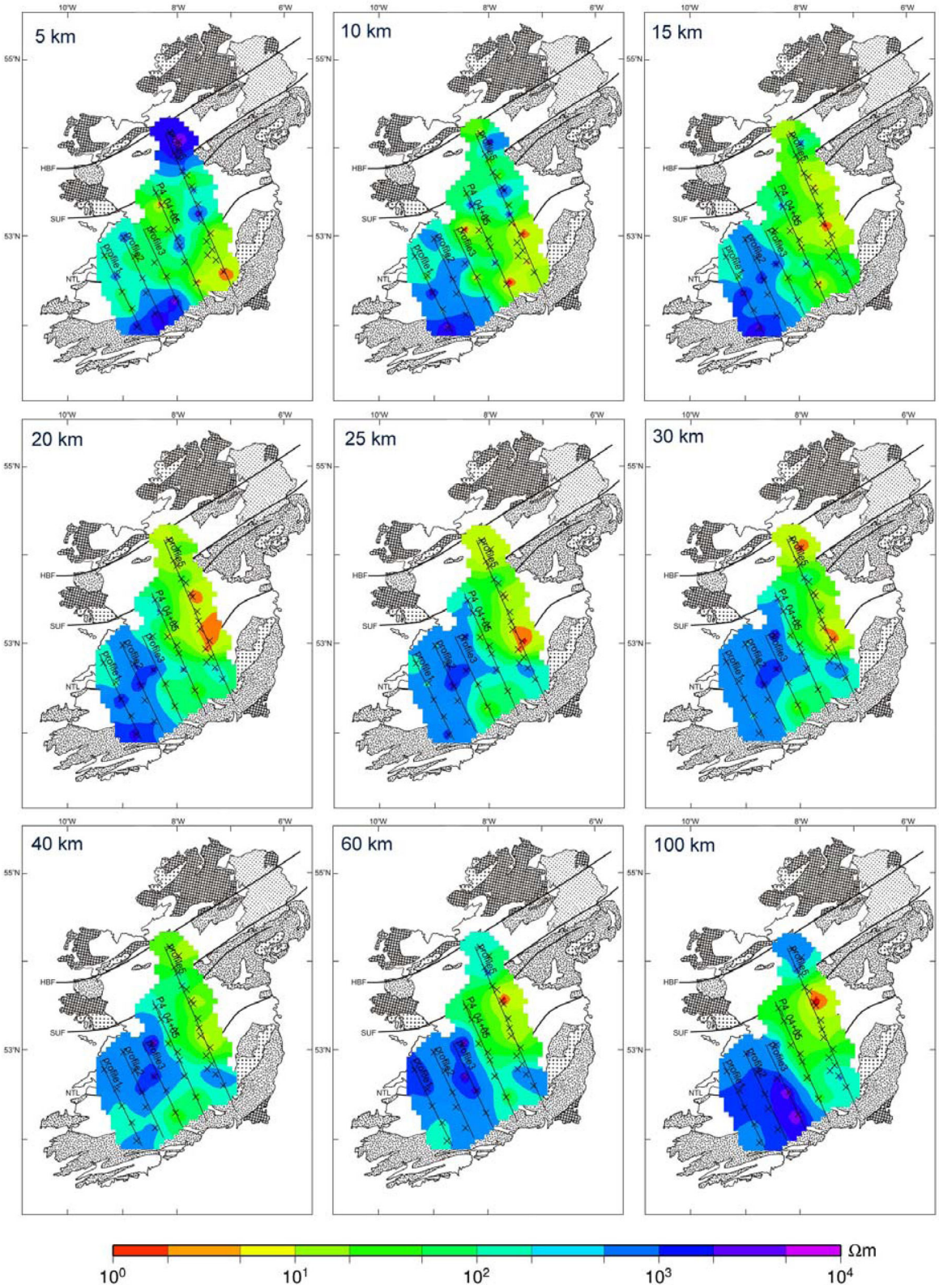

Figure 9. Depth sections obtained from geo-electric sections along all five profiles in Ireland; HBF, Highland Boundary Fault; SUF, Southern Uplands Fault; NTL, Navan Tipperary Lineament.

39 sites; Figs 10(a) and (b) illustrate this fit at six representative sites, one site from each profile. The data fits to the XY component curves and the YX phase curves are generally good, whereas the YX apparent resistivity curves exhibit a similar shape with lower magnitude (Fig. 10a) indicating static-shift effects (Jones 1988; Jones 2011). The XX and YY responses of apparent resistivity and phase are shown in Fig. 10(b). The regional features obtained with the 3-D forward model (Fig. 11) are reasonably comparable to

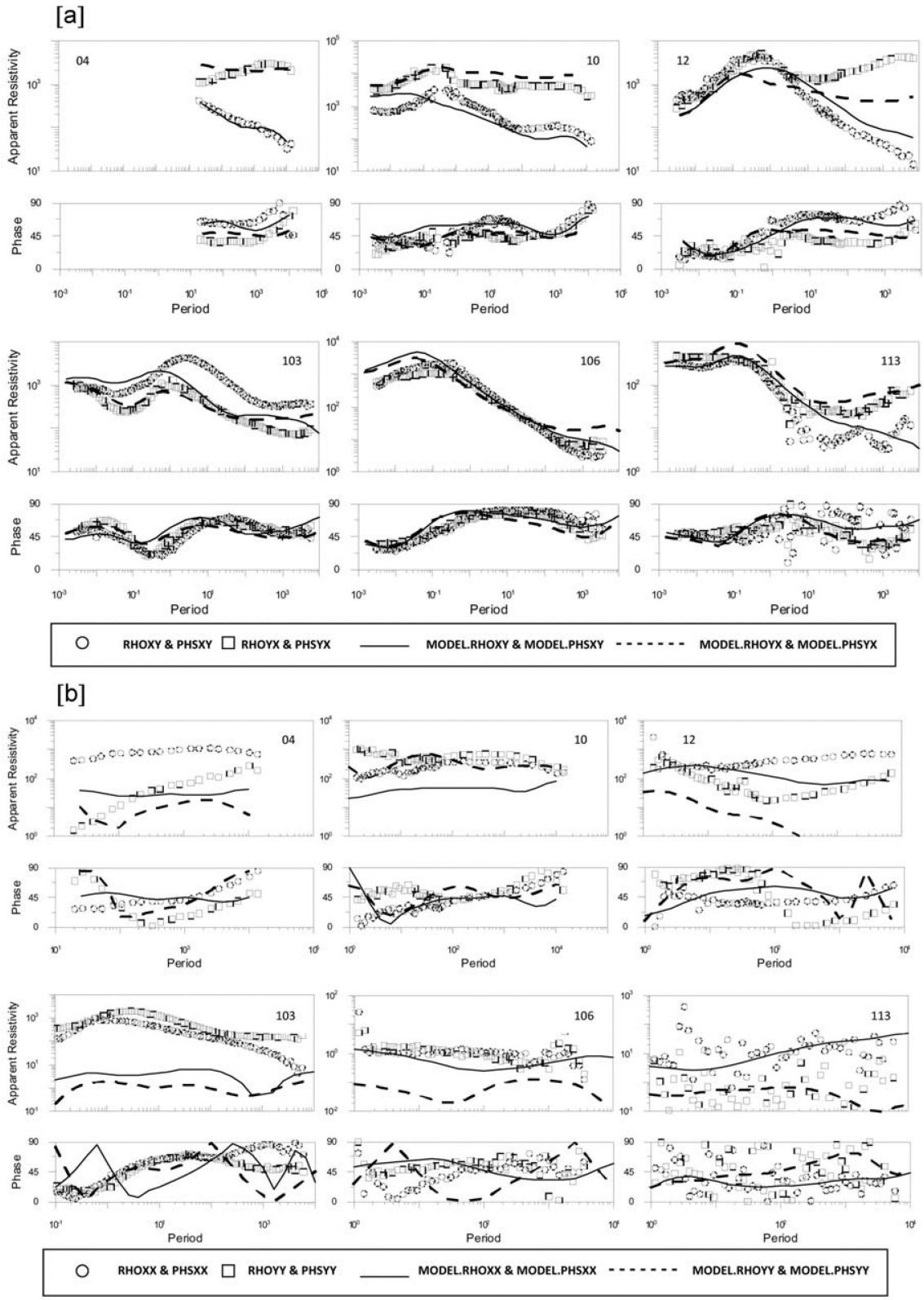

Figure 10. (a) Representative sites showing observed data (XY and YX, resistivity and phase) and 3-D forward model fit to the data points, (b) XX and YY responses for observed and 3-D forward model fit.

those obtained in the 2-D inversions. The final model is illustrated in Fig. 11 for various depth slices, and it also shows that the eastern half of Ireland is conductive whereas the western part is resistive throughout the entire lithosphere to 100 km.

3-D INVERSION MODELS

To assess the validity and robustness of the 3-D forward model we performed two different types of 3-D inversion: a constrained

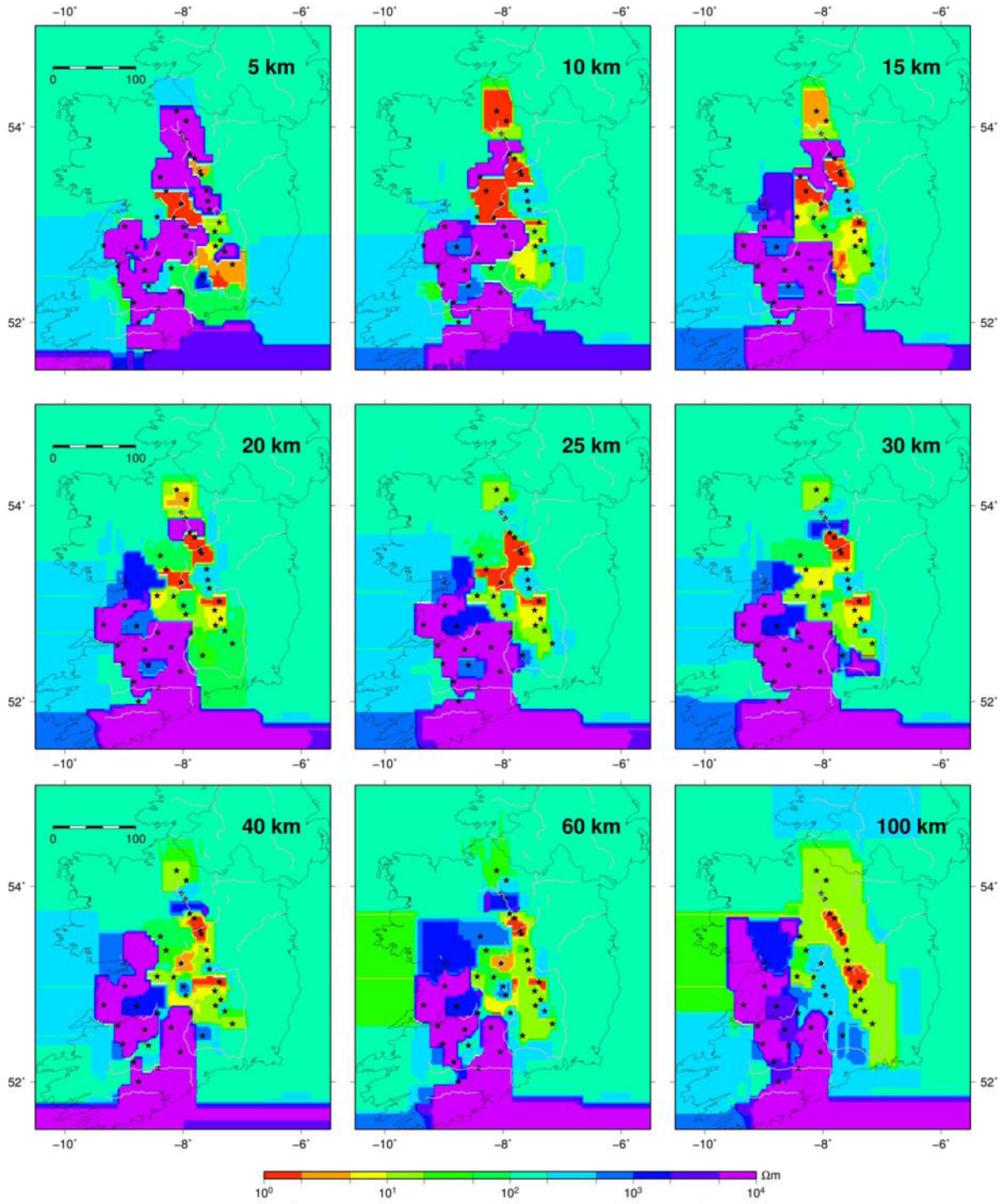

Figure 11. Horizontal slices obtained by 3-D forward model at different depth planes.

3-D inversion based on the final 3-D forward model shown in Fig. 11, and an inversion study starting from homogeneous half space models. For both studies we used the modular modelling and inversion package ModEM (Egbert & Kelbert 2012) in its parallel version (Meqbel 2009). The constrained inversion run using the 3-D forward model as the starting and prior model resulted in only some minor adjustments in the subsurface conductivity structure. The final data fit with error floors settings to 5 per cent for individual off-diagonal, 10 per cent for individual diagonal impedance values and 0.02 for the vertical magnetic transfer functions was satisfactorily with an rms value of 2.3.

Since the constrained inversion results cannot be regarded as an objective and unbiased assessment of the 3-D forward model, we therefore focus on the inversion study starting from homogeneous half space models. However, as we will show, this study

demonstrated that, to a large degree, the 3-D forward model represents an acceptable explanation of the observed data.

In preparation for 3-D inversion, we synthesized the MT data from different instruments and processing methods to obtain an MT data set with 46 consistent periods. For the starting and prior model of the 3-D inversion we used a homogeneous half-space of 500 Ωm, including the ocean pre-set to 0.3 Ωm. The grid had a size of 44 × 59 × 81 cells; the first vertical cell was 25m thick increased by a factor of two towards depth. The horizontal mesh was chosen to be consistent with the 3-D forward study; however tests with different discretization did not change the inversion results significantly. Since the regularization of the ModEM inversion scheme penalizes deviations from a prior model as part of the model update search, we needed at least a two-step inversion run to make sure the inversion model develops farther away from an homogeneous half-space. The final model was re-started three times using the model of the previous inversion run as the starting model. Typically these runs complete because a moderate decrease in misfit is accompanied by a significant increase in model complexity. When restarting the inversion runs, significant improvements in data fit were again possible. For the 3-D inversion, error floors were set individually to 5 per cent for the off-diagonal and 10 per cent for the diagonal impedance values and to 0.02 for the vertical magnetic transfer functions. The inversion was performed with isotropic model covariances of 0.2 in each direction (X, Y and Z). The data fit of the starting model half-space (with ocean) yielded an rms of 48, which was reduced within the course of the inversion procedure to a value of 1.98. In addition, we applied some resolution tests for certain conductivity features present and found to be robust in the 2-D inversion results that did not show up in the 3-D inversion. We included, for example, the UMC conductor beneath profile IV (Fig. 8) as a 20 km broad *a priori* feature into the inversion result between 50 and 80 km depth (Fig. 12 slice of 60 km depth). This improved the data fit at stations 104–106 and 25 resulting in a final rms of 1.91. We will discuss these tests in more detail when comparing features below.

DISCUSSION OF 2-D AND 3-D INVERSIONS AND 3-D FORWARD RESULTS

In the following we will compare the modelling and inversion results of three different approaches: 2-D inversion, the 3-D forward model derived from the 2-D models, and the 3-D inversion.

While it is rather well accepted that generally 2-D inversions can only be regarded as a first order approximation of the actual, usually more complex, subsurface conductivity structure, they are still superior in terms of possible discretization of the subsurface (e.g. Siripunvaraporn *et al.* 2005; Meqbel 2009). Due to the much denser meshes feasible for 2-D inversion, these models typically result in more detailed conductivity images. Also, computational cost of 3-D inversions is prohibitively high for conducting hypothesis and resolution tests to the same extent possible in 2-D inversion. It is beyond the scope of this paper to discuss the trade-off between structural details and artefacts introduced by the simplifying and not entirely satisfied 2-D assumptions, but pertinent to the work is that 2-D inversion models can be biased as off-profile features might be mapped as artificial conductivity features beneath the profiles (e.g. Ledo *et al.* 2002; Ledo 2005). This implies that the mislocated features might have made their way also into the 3-D forward model, as it is, to a large extent, based on the 2-D results. Therefore, the 3-D forward model cannot be regarded as completely independent of the 2-D results, but nevertheless it is able to account for the regional conductivity contrasts in Ireland, such as the surrounding oceans and that the modelled conductivity anomalies are not 2-D in a strict sense as changes can be observed between profiles. Otherwise, 3-D inversion does not consequently result in superior, that is more realistic and veracious, conductivity models. Tietze & Ritter (2013) illustrated that even though 2-D inversions of several profiles across the San Andreas Fault yielded a robust conductivity anomaly in the lower crust, 3-D inversion was initially not able to recover it. Only the introduction of *a priori* information or rotation of the underlying coordinate system led to correct recovery of a pronounced regional 2-D structure.

Against this background, we show depth slices of the 3-D inversion result (Fig. 12) which we compare to depth slices of the forward model. In general, areas with high or low conductivities correlate in a relative sense. One major difference between the two 3-D models is the chosen background conductivity, which was 100 Ωm for the forward model and 500 Ωm for the inversion model. The choice of a homogeneous half-space of 100 Ωm for inversion resulted in a slightly rougher image with more extreme conductivity values. This could explain why resistors are less resistive and conductors less conductive in the 3-D inversion result, or simply as a consequence of the Tikhonov smoothing regularization trade-off parameter employed in the inversion objective function.

For a trial-and-error approach, which forward modelling does represent, it is rather impossible to include small scale features at, for example, depths of ≤15 km (Fig. 11 upper row), thus 3-D inversion therefore comprises more structural variability. However, in the upper 15 km (Fig. 11 upper row), most of the highly resistive and conductive zones are also present in the inversion model (Fig. 12 upper row). At lower crustal depth levels both the forward (Fig. 11 middle row) and inversion (Fig. 12 middle row) models are in good agreement with each other, whereas at deeper layers horizontal smoothing is obviously greater in the 3-D inversion model (Fig. 12, bottom row) compared to the 3-D forward model (Fig. 11, bottom row). Whereas in the 3-D forward model only higher resistivities were included in the southern part of the grid, the 3-D inversion model additionally infers more resistive structures in the northern part of Ireland outside the area of site coverage.

One of the major differences between 2-D and 3-D inversions is the parameters to be fitted: whereas 2-D inversions usually fit apparent resistivities and phases, 3-D inversions focus on the individual complex-numbered impedance tensor elements. Since they become very small in the case of conductive features, it can easily occur that such a structure, although the MT method is more sensitive to conductors, is missed. This might also be the reason why one of the pronounced deep conductivity anomalies (UMC) was initially not present in the initial 3-D inversion results. Only after including this structure as *a priori* information, the restarted inversion run kept this feature by reducing the rms at the same time. Detailed inspection of stations 103–106 and 25 confirmed that the data fit to the long period data was improved with its presence.

A detailed overview on the obtained data fit between the 3-D inversion model (Fig. 12) and the data are presented in Fig. 13. The rms values are calculated for various subsets of data components and period ranges. The upper row of Fig. 13 shows the total rms for the full impedance tensor and the vertical magnetic transfer functions (top left) and separately for magnetic transfer functions (top centre) and impedances (top right) accumulated for all periods. In the middle row, we present the rms values of both diagonal (centre left) and the individual off-diagonal impedances (centre middle and centre right) for the entire period range. The lower row gives

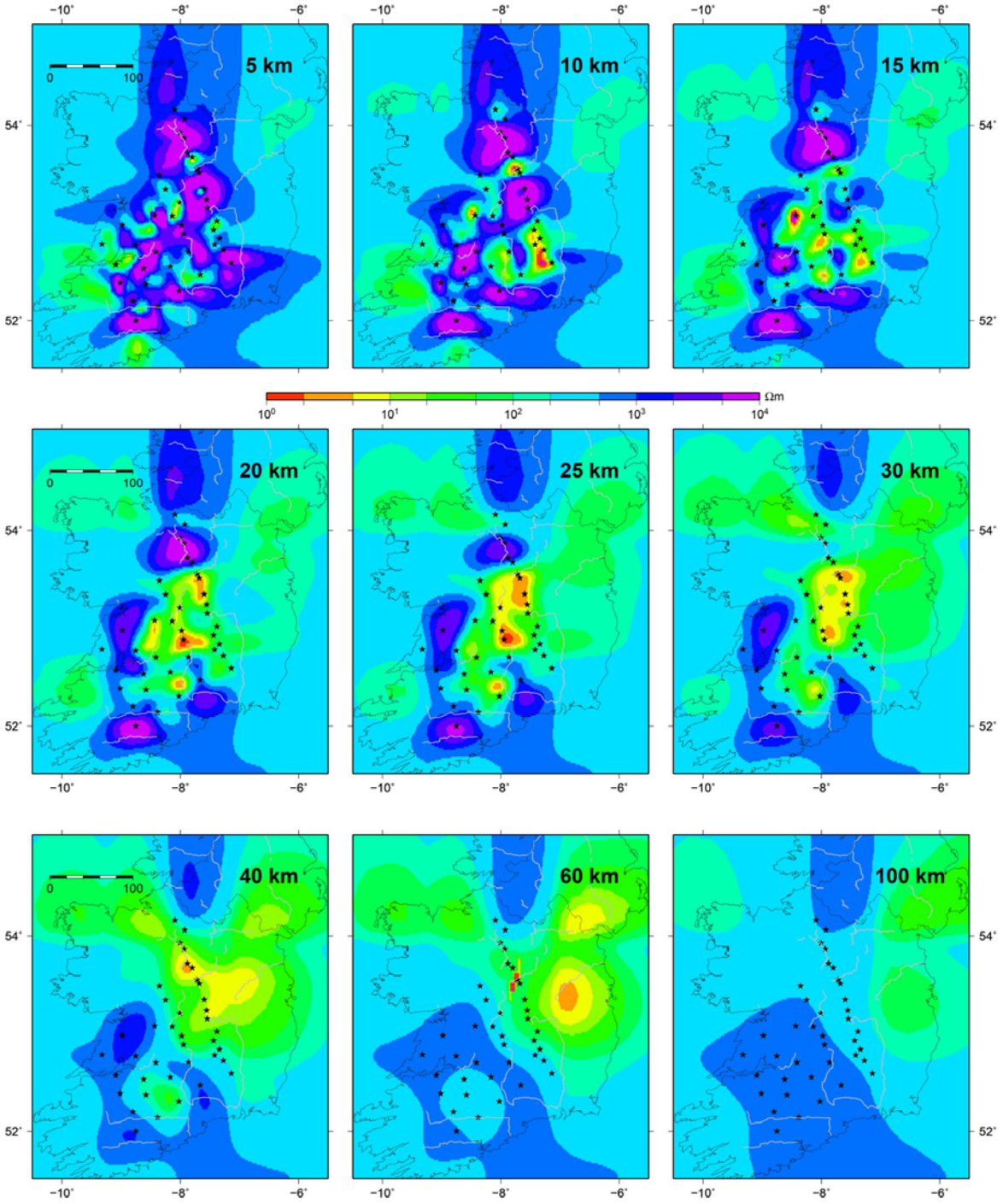

Figure 12. Horizontal slices showing the electrical conductivity distribution of the 3-D inversion model at the same depth as in Fig. 11. We used a homogeneous half-space including the ocean as starting and prior model in the modular ModEM 3-D inversion package (Meqbel 2009; Egbert & Kelbert 2012).

accumulated total rms values (impedances and Hz) for different period ranges. Only a few stations appear to have a significantly worse data fit than the average. In general, the total rms, based on the data fit for all individual impedances and vertical magnetic transfer functions, is below 2; there are a few sites with slightly higher (yellow colours) values. The breakdown of total rms into its contributions from different impedance tensor components (Fig. 13 middle row) or period ranges (Fig. 13 bottom row) shows some variations across the array, however, large areas where the 3-D inversion model systematically cannot explain the data (rms values greater than ∼3) are not obvious.

Fig. 14 provides sections of the 3-D inversion model along the 2-D profiles. Most of the prominent and labelled conductivity anomalies from the 2-D inversions (see Fig. 8) are also present in the 3-D inversion model. Profile I (Fig. 14) includes both resistors R7 and R8, but now with slightly modified shapes. Of the tectonic features, the NTL seems to correlate with the eastern boundary of R7, while at shallow depth (<1 km) the KMFZ seems to limit R8 beneath

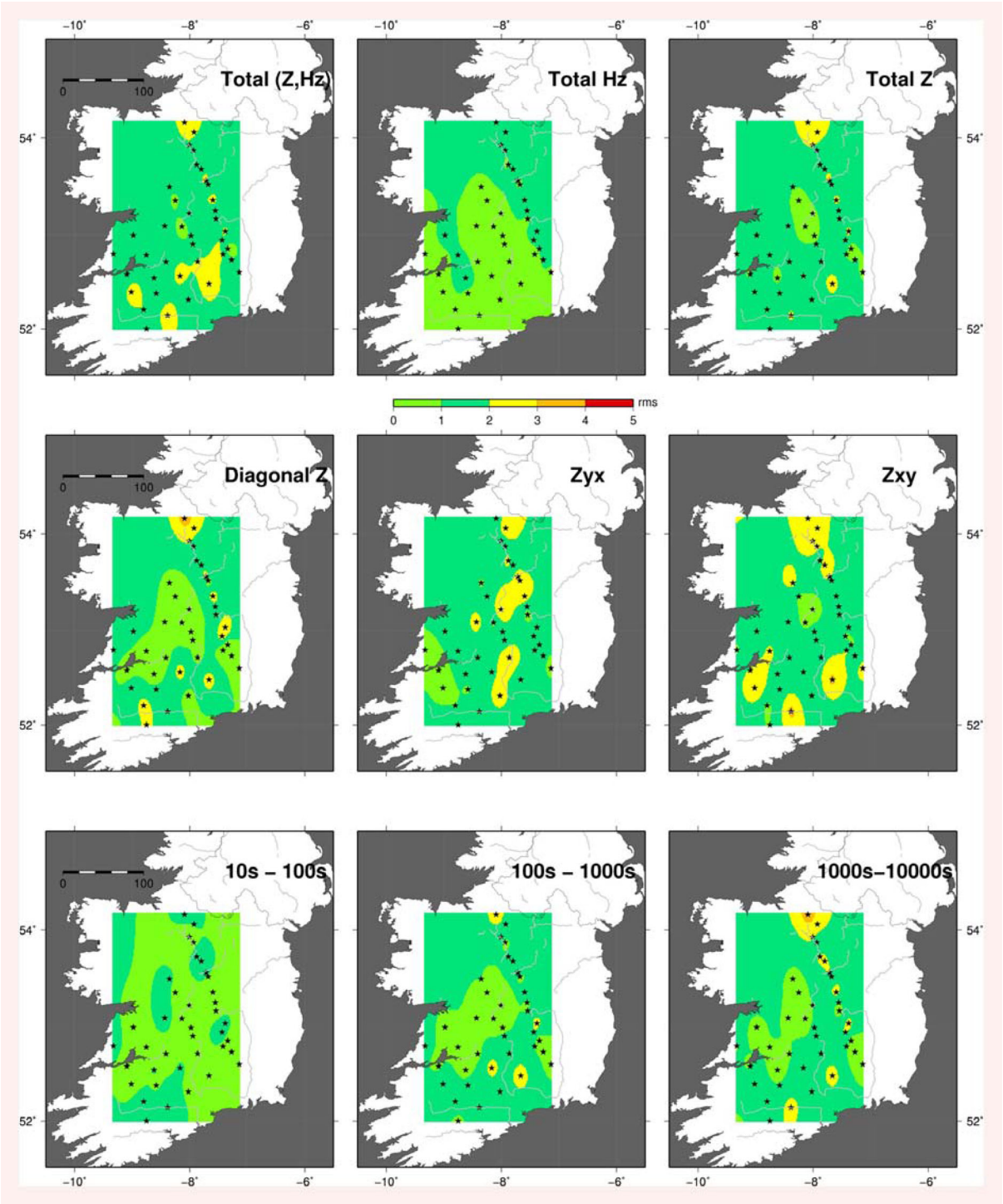

Figure 13. Maps of rms values for the 3-D inversion model (Fig. 12) for different data components and period ranges. The upper panel shows the total rms for the full impedance tensor and the vertical magnetic transfer functions (left) and separately for impedances (middle) and magnetic transfer functions (right) accumulated for all periods. In the middle panel we present the rms values of both diagonal (left) and the individual off-diagonal impedances (middle and right) for the entire period range. The lower panel gives accumulated total rms values (impedances and Hz) for different period ranges. In general, larger areas for which the MT data is not explained by the 3-D inversion model are not obvious.

which high resistivities continue farther south. Conductivity anomaly C7 occurs in both the 2-D and 3-D inversions, although the higher conductivities dipping beneath R7 and R8 are not as similarly pronounced in the 3-D model as in the 2-D result. Beneath site 02 both inversions sense a very shallow small scale high conductivity anomaly but which exhibits higher conductivities in the 3-D case.

Profile II of the 3-D inversion model includes resistors R5 and R6, although suggesting a continuation of the resistive zone towards the NW, cutting conductor C6 at a depth of 10 km. In return, the 2-D inversion implies deep-reaching conductivities in this area. Interestingly though, the NTL seems to define a southern limit to the shallow resistive block R5, which would be in contrast to profile

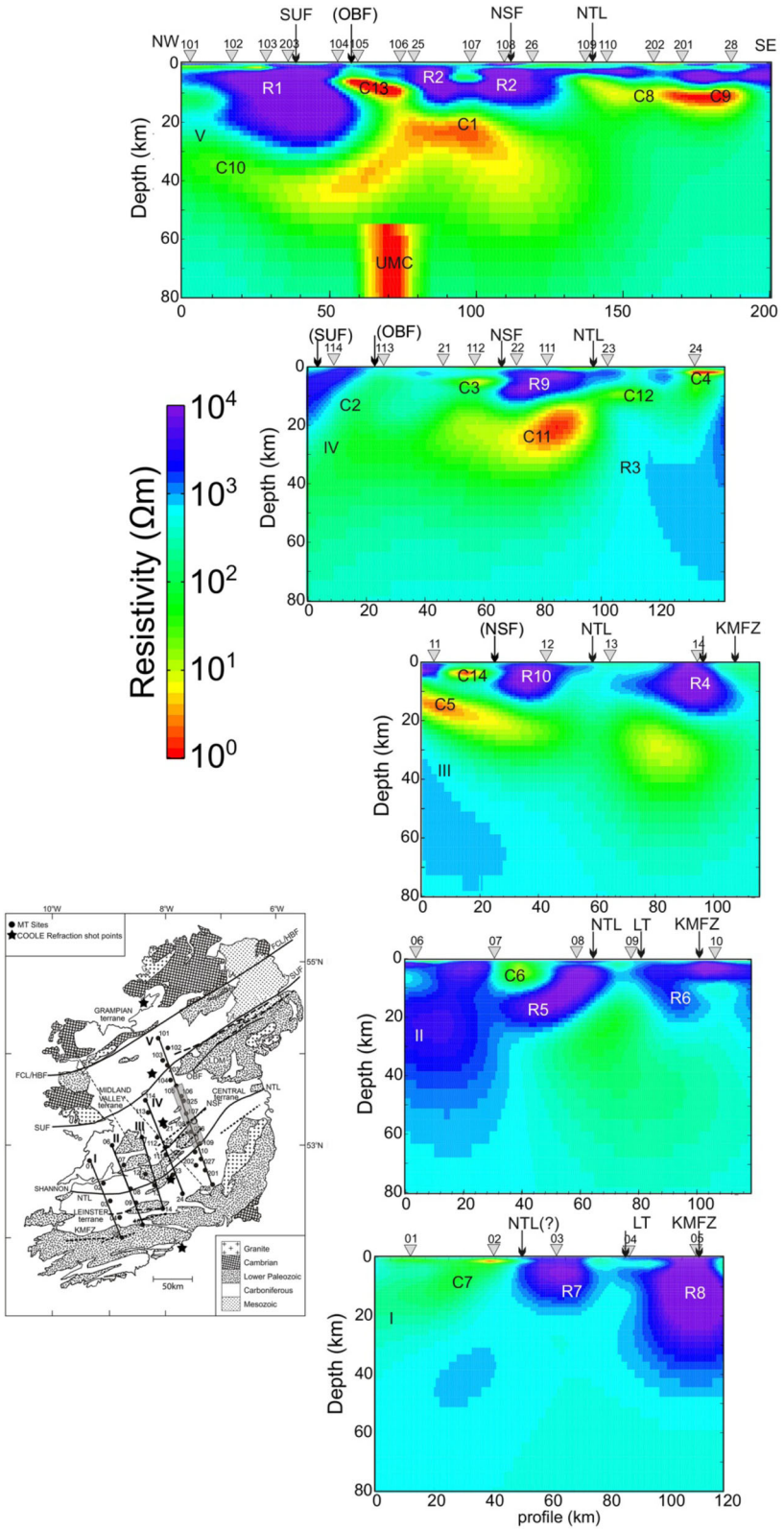

Figure 14. 2-D conductivity sections across the Iapetus Suture Zone along all five profiles in Ireland obtained from 3-D inversion of the full MT impedance tensor and the vertical magnetic transfer functions. The detailed discussion and comparison to the 2-D sections of Fig. 8 can be found in the text. The surface expression of tectonic structures is indicated by arrows. Gray (UK English spelling?) colours are used if the position is inferred from an extrapolation of outcrops. SUF, Southern Uplands Fault; OBF, Orlock Bridge Fault; NSF, Navan Silvermines Fault; NTL, Navan Tipperary Lineament; KMFZ, Killarney Mallow Fault Zone; LT: Leister Terrane.

I but more consistent with profiles II–IV. The resistive body R6 along profile II appears sandwiched between the Leinster terrane boundary and the KMFZ.

Similar limiting structures might be possible for the resistor R4 in profile III, while R10 is sandwiched between the NTL and an extrapolation of the NSF. This is in contrast to the 2-D inversion model (Fig. 8) that shows decreased shallow resistive blocks and higher conductivities dipping southward from near site 12, being underlain by high resistivities again. However, the general behaviour of deep structures (conductor and resistor below) is comparable again in the 3-D model, albeit with depth range differences. Based on the rms values (see Fig. 13), we do not have any indication that the conductivity structures observed in the 3-D model result from flawed data fits. When considering the geological map (Fig. 1), which shows more 3-D structures and therefore off-profile features, it is likely that they affect the 2-D inversion along profile III.

The shallow conductive zone C14 close to site 11 in the 3-D inversion seems to be connected north-eastward with C3 on profile IV. In the 2-D inversion model we can identify a similar feature further south. Given the distance between the stations along this profile, such shifts in position are not surprising though.

The resistive block (R9) between the tectonic features NTL and NSF is consistently resolved in both the 2-D and 3-D inversion models. Several zones of high conductivities C2-C4 in the upper crust appear to have their equivalents also in both inversions; however, C12, which does not occur in the 2-D inversion, is present in 3-D and shows a connection to C8 and C9 of profile V. An additional conductor C11 is exhibited by the 3-D inversion that starts north of NTL and has a weaker expression up to the northern end of the profile and thus connects again to profile V.

Profile V is by far the one with the most structure in 2-D. In 3-D we observe very similar features, for example, R1 and R2 as well as C8 and C9. The OBF appears to correlate spatially with a shallow zone of high conductivities (C13 in 3-D model, Fig. 14), which clearly dips south-eastward and is disrupted from a deeper subhorizontal conductor C1. The 2-D result (Fig. 8) does not recognizably show this disruption, but here the structures seem to merge with C1 that stretches from the NSF to the OBF and continues farther north as conductor C10. In return, the 3-D model shows C1 bound by the NSF and the SUF and show a continuation of less conductive material farther north.

DISCUSSION AND INTERPRETATION

The 2-D inversion models and depth sections of the 3-D inversion model along the five profiles (Figs 8, 9, 11, 12 and 14) show a large range of electrical resistivity of more than five decades, from less than 1 Ωm to well over 10 000 Ωm, for rocks in Ireland's crust and upper mantle. The NW part of profile V exhibits a highly resistive body (Rl; Figs 8 and 14) below a layer of sediments of relatively moderate resistivity (150–500 Ωm) and thickness of approximately 2 km which reaches up to the surface between stations 203 and 104. The sediments that lie in the Midland Valley terrane are predominantly Carboniferous limestones and Devonian sandstones in the Carrick syncline (stations 101–103). Within these sediments we identify a conductive layer with resistivities as low as 15–50 Ωm, which may be due to shale content in these sediments. Philcox *et al.* (1989) suggested, from stratigraphic data in the Midland Valley terrane, that Lower Carboniferous limestones rest unconformably on Lower Devonian sandstones. Support for such a geological setting is provided by the COOLE seismic refraction profile that reveals a layer of *P*-wave seismic velocity 5.6 km s^{-1} (Lowe & Jacob 1989), typical of Carboniferous limestones and Devonian sandstones.

Pertaining to profile V, the highly resistive layer (feature R1; Figs 8 and 14) was interpreted previously by Rao *et al.* (2007) as Ordovician metabasites and mafic greywackes. The feature is not sensed on the other profiles due to their limited northern extent. The two resistive blocks (features R2; Figs 8 and 14) in the centre of the profile were interpreted by Rao *et al.* (2007) as Caledonian granites emplaced in the upper crust during the late Caledonian Igneous activity. These two resistive blocks are also seen below the northernmost stations on profile IV in the 2-D inversion model, whereas both the forward and inversion 3-D models exhibit generally resistive shallow subsurfaces but with less pronounced anomalies. In the Central terrane, MT stations south of the OBF and north of the NTL (Fig. 1) show the top layer having a thickness of about 1–4 km with resistivity of 300–3000 Ωm. It is difficult to discriminate electrically between sedimentary and volcanic rocks beneath this locality due to the high resistivity of the sedimentary Carboniferous limestones in this region. A similar resistivity was been reported by Brown & Whelan (1995). Sevastopulo (1982) inferred that these limestones had initially a high porosity, but that porosity was rapidly reduced with the deposition of micritic internal sediments and precipitation of marine fibrous cement. A highly resistive layer is defined in the Leinster terrane (southern part of NTL) across profiles I, II, III and IV (R3-R4 & R6-R8; Figs 8 and 14) that is likely to be due to prevailing Late Ordovician volcanic rocks and the Leinster granite that lies below them. The high resistivities may indicate low porosity or lack of fluid connectivity that may be consistent with various rock types in the Leinster terrane. One such possibility is Duncannon Group's thick sequences of intermediate to acid volcanic rocks, which crop out in the south of the Leinster terrane. However, these are restricted to the shallow surface. The other possibility is Old Red Sandstone strata with silica in its pores during high stain rates, south of KMFZ deposited in the Munster basin (Brown *et al.* 2003). The Inch Conglomerate may also support the interpretation of resistors R6 and R8. The Leinster granite is also known for its high resistivities in this part of the study region. The resistor R5 on Central terrane may be due to Silurian ferromagnesian rich greywackes.

The Central terrane south of the SUF and north of the NTL (Fig. 1) is identified as an anomalous zone throughout the whole crust (Lowe & Jacob 1989; Rao *et al.* 2007). Figs 8 and 14 show a very high conductivity zone with its top at depths of ∼5–20 km and resistivity of 1–10 Ωm (C1-C5; Figs 8 and 14), with the exception of C6 and C7 with somewhat higher resistivities of 30–100 Ωm and depths of 5–10 km. As shown in Figs 8 and 14, the high conductivity zone becomes shallower as one traverses from east to west across Ireland.

The main ISZ conductor is bounded to the north and south by two known faults (OBF & NTL; Fig. 1) where the conductor rises to a depth of 5 km below the surface. From their MT study in south-western Scotland, Tauber *et al.* (2003) defined a similar highly conductive block at a depth of 4 km along strike. The main conductor between the OBF and NTL faults closely resembles the broad crustal change inferred as shallowing of wide-angle reflectors towards the north (Lowe & Jacob 1989) in the region of the ISZ.

The southernmost stations on profiles I and II show a subvertical highly resistive layer (features R6 and R8). This region lies on the Variscan orogenic belt that extends from Ireland into Great Britain and further eastwards (Matte 1986). The southern part of the Killarney Mallow Fault Zone (KMFZ; Fig. 1) is usually taken geologically as the northern margin of Variscan deformation.

Although the MT data at short periods at most of these stations were discarded, due to electric fence noise disturbance, the long period data are relatively free from noise and are of good to high quality; they clearly indicate the resistive body (R6 & R8; Figs 8 and 14). Similar resistive structures were also inferred in prior MT studies (Brown *et al.* 2003). Sites 10 and 04 are located in the vicinity of a mapped fault zone, and Landes *et al.* (2000) modelled the shallow upper crustal basement with a thin sedimentary layer at these stations. The resistive structure (>10 000 Ωm) observed in our studies implies high grade metamorphic crystalline basement comprising low porosity volcanic rocks in the region.

The first-order and robust feature in the 2-D depth sections (Fig. 9) and 3-D forward and inverse modelling (Figs 11 and 12) of the middle crust to the upper mantle is that the eastern part of southern Ireland below profiles IV and V is significantly more conductive than the western part below profiles I and II. The resistive-conductive contact zone is located in central Ireland in between profiles II and III. Additional geophysical data sensitive to other petrological-geophysical parameters also display this strong east–west asymmetry. Seismic refraction studies (Jacob *et al.* 1985) along the inferred ISZ recorded lower seismic velocities (5.4 km s^{-1}) in the eastern part of the profile than in the western part (6.0 km s^{-1}). Those authors also noted the absence of the low velocity zone (LVZ) in the western part. Hauser *et al.* (2008) employed seismic shear-wave wide-angle reflection data across the southwest of Ireland and, based on Poisson's ratio in the upper part of the crust to a depth of about 15 km, they suggested the presence of high silica content rocks (up to 75 per cent) in the region. It is also noted that the lower part of the crust is also silica rich (∼64 per cent), as supported by petrological and geochemical data on xenolith samples (van den Berg *et al.* 2005). The silica richness in western Ireland is also corroborated by faster *P*-waves (negative traveltime anomaly) from the tomographic study by Wawerzinek *et al.* (2008). This strongly supports our observation that the crust of western Ireland is highly resistive. In contrast with this, eastern Ireland, with slower *P*-waves and the presence of LVZ (Jacob *et al.* 1985), supports our observation of higher conductivity. The high conductivity in eastern Ireland may be due to the shale and sulphidic material within the sedimentary accretionary wedge at the Iapetus subduction zone. As the Iapetus Ocean closed and sutured, in the east there was deposition of conducting sediments and subsequent subduction deep into the crust, whereas in the west either that material was not available for subduction, or it was not subducted deeply into the crust and has subsequently been eroded. In either circumstance, the tectonic processes varied along strike of the orogeny during Iapetus Ocean closure and continental suturing. Finally, the recent surface wave anisotropy study of Polat *et al.* (2012) shows strong east–west asymmetry in seismic velocity for lower crustal and upper mantle depths. Intriguingly, the shaded Bouguer anomaly gravity map of Ireland (Readman *et al.* 1997, their fig. 5) does not exhibit obvious east–west asymmetry.

High conductivity at crustal depths can be caused by many factors, such as saline water, partial melt, sulphides, iron oxides and graphite (Frost *et al.* 1989; Jones 1992; Duba *et al.* 1994). High conductivity in the tectonically non-active paleo-orogenic regions is generally correlated with magnetite-rich serpentinization or metamorphosed graphitic/sulphidic sediments (Weckmann 2012). It seems most likely that the high conductivity we observe is due to the occurrence of low-grade metamorphosed graphitic sediments in Palaeozoic suture zones. Early Ordovician time was characterized by an abundance of black shales (Dewey 1988), and during the Ordovician-Silurian times, abundant black shale deposition occurred on the drowned carbonate shelf margins of the narrow, closing Iapetus Ocean at tropical latitudes (Leggett 1978; Klemme & Ulmishek 1991; Trabucho-Alexandre *et al.* 2012). These shales represent a major component of flysch within accretionary sedimentary wedges at subduction zones. As illustrated in Fig. 8, we interpret the high conductivity at upper to lower crustal depths as due to black shales, with possibly sulphides in addition, as the likely cause. Rao *et al.* (2007) previously proposed the central high conductivity zone as the one composed of metamorphosed graphitic sediments with its sulphide content in reducing conditions.

Others have also appealed to this explanation in the interpretation of their data in other locations. Hjelt & Korja (1993) summarized the upper and middle crustal conductivity in Europe in different tectonic regions including Variscan-Caledonian Europe and the ISZ, as due to graphitic-sulphidic rocks with metamorphosed graphite-bearing rocks. Electromagnetic imaging in SW Iberia across the Variscan orogen (Pous *et al.* 2004) discovered a highly conductive zone (10–50 Ωm) at middle to lower crustal depths interpreted as a zone of interconnected graphitic sediments.

We find that the high conductivity in the centre of the profiles reduces to moderate conductivity in the south western part of Ireland, with a resistivity of 50–100 Ωm at upper to middle crustal depths. Similar results have also been reported by Korja *et al.* (2008) in the Central Scandinavian Caledonides, with resistivity ranging from 0.1 Ωm in the west to 100 Ωm in the east. Those authors attributed the change in resistivity to maturity of the shales, with conductivity increasing with maturity from semi-anthracitic to anthracitic.

Geochemical analyses of shale samples from selected belts within each terrane by Ryan *et al.* (1995) support our interpretation. The analyses showed that the shales from the central and northern belts (LDM, Fig. 1) have low maturity, whereas those from southern part and the Leinster belt have relatively high maturity. In our study, although it is difficult to find exact spatial correspondence with the litho-geochemical analysis of Ryan *et al.* (1995), the change in resistivity in the western part of Ireland is attributed to the similar processes, as discussed similarly by Korja *et al.* (2008).

Figs 8 and 9 show a prominent conductor in central Ireland at upper mantle depths of 60 km and deeper on profile V below the stations 105–107, that is not seen beneath the other profiles. Landes *et al.* (2007), based on teleseismic shear wave receiver functions (RFs), suggested that the Lithosphere-Asthenosphere Boundary (LAB) is at a depths 85 ± 5 km to the south and 55 ± 5 km to the north of Ireland. Wawerzinek *et al.* (2008) modelled a LVZ at depths of 60–90 km in central Ireland and interpreted this as the onset of thinning of the lithosphere caused by upwelling plume material compared to the lithospheric depth of 90–120 km in western Ireland. Such lithospheric thinning is impossible, as it would result in 2 km of uplift in northern Ireland, as well as gravity and geoid signature, none of which are seen (Fullea *et al.* 2014; Jones *et al.* 2014). Nonetheless, Landes *et al.* (2007) mapped a mid-lithospheric discontinuity that requires explanation.

More recently, using joint inversion of teleseismic *P*-wave delay times and the long wavelength gravity of Ireland, O'Donnell *et al.* (2011) delineated a number of low velocity and density heterogeneities at depths greater than 50 km. Those authors interpreted these anomalies as related to either terrane accretion associated with Iapetus Ocean closure, or frozen Iceland plume-related magmatism, or a combination of both of these causes. The impetus for the plume hypothesis came from the work of Al-Kindi *et al.* (2003) and Arrowsmith *et al.* (2005) who found low *P*-wave velocity below the

British Isles and northeastern Ireland, and suggested that these were related to hot upwelling material of the Iceland plume.

High conductivity at upper mantle depths can be caused by a number of factors. In regions of higher heat flow or at depths likely beyond the LAB, it is widely accepted that high conductivity in upper mantle is an indication of the presence of partial melt or hydrous fluids (Shankland & Waff 1977). High conductivity may also arise due to amorphous graphitic carbon (Duba & Shankland 1987) or hydrogen diffusion in bound water (Karato 1990) although the details of the latter are highly contentious between the different laboratories making the measurements on hydrous samples of mantle minerals (Jones *et al.* 2012). Regardless of the water model chosen however, none will give such low resistivities (<5 Ωm) for reasonable amounts of water. Hjelt & Korja (1993) described the causes of upper mantle conductivity in different tectonic frameworks and, in a comprehensive study, Jones (1999) reviewed the available geophysical processes in an effort to image the continental upper mantle.

The high conductivity anomaly in the upper mantle of the present study region is below a zone of relatively high heat flow of 52–87 mW m^{-2} (Brock 1989) and inferred thermal anomalies (Wawerzinek *et al.* 2008) of 100–180 °C. In view of all of the above causes, the upper mantle conductor may not be interpreted as due to thinning of the lithosphere in the region, since there is no indication of change in topography in central as well as northern Ireland that might be generated due to the lithospheric thinning (O'Donnell *et al.* 2011). In the northern part of Ireland, numerous remnants of volcanic activity are found that belong to the British Tertiary Volcanic Province (Preston 2009), particularly the basaltic Antrim plateau, and can be explained by the spreading head of proto-Iceland plume whose melts ascended to the surface along fracture zones (Cliff *et al.* 1998). The Iceland plume-related magmatic intrusion may be the cause of the high conductivity that we find at upper mantle depths below the stations 105–107 through introduction of conducting interconnected material, in much the same manner as the mantle beneath the Bushveld Complex of the Kaapvaal Craton is highly conducting as a consequence of Bushveld Paleo-Proterozoic magmatism into Archean cratonic lithosphere (Evans *et al.* 2011). The nature of the conducting material remains elusive at present.

Although the present study has highlighted the conductivity changes across Ireland at the regional level, it would be interesting to investigate the detailed geo-electric structure of the ISZ with high-resolution MT measurements in an effort to improve the understanding of the geodynamics of this important suture zone.

CONCLUSIONS

We conducted a 3-D electrical investigation of the ISZ in Ireland comprising a MT survey of 39 broad-band sites, many supplemented by long period acquisition, organized along five approx. NNW-SSE profiles. Modelling and inversion of the data was undertaken in both 2-D and 3-D. The 2-D inversion models and 3-D forward and inversion models of the MT data revealed the following salient features:

(1) Highly resistive bodies in the upper crust are most logically associated with Ordovician volcanic rocks in the NW part of the profiles. Across the centres of the profiles, Caledonian granites emplaced during the late Caledonian igneous activity appear to cause the observed high resistivities. Similarly, the observed high resistivity across the SE part of the profiles is interpreted as that due to Leinster granite in the region.

(2) The geologically and geophysically recognized major faults (OBF, NSF, NTL) are identified as resistive-conductive contact zones. The causative factors for shallow conductors observed in all profiles include particularly black shales. Although there is an indication of a dipping resistor at the KMFZ, it is not clearly resolved due to the sparse data in that region. Using the conductivity models in the study region, we infer that the southern boundary of the ISZ lies between the NSF and NTL faults.

(3) Observed across all profiles, we interpret the high conductivity at middle to lower crustal depths as metamorphosed graphitic sediments rich in sulphide content, and they correlate well with the LVZ inferred from seismic studies across the central and eastern part of Ireland.

(4) The rise in resistivity, from low in the eastern profiles to relatively high in the western profiles, as revealed in 2-D depth sections and 3-D forward and inverse modelling, is related to the composition of the rocks that are dominated by the matured shales in the eastern and central part and volcanic rocks in the western part of the study region. This change in physical properties is also observed in seismic models, and speaks to the variation in the depositional processes along strike of the ISZ as the Iapetus Ocean closed and the Laurentian and Avalonian continents sutured. Either there was little sediment feeding the orogeny to the west, or the geometry of collision was such that sediments were not subducted deep into the crust in the west but were closer to the surface and have been subsequently eroded.

(5) The conductor at upper mantle depths close to 60 km in the profile V, underneath the stations 105–107, is problematic to interpret. Given its low resistivity we can exclude hydrogen diffusion. We note that it lies at a similar depth as the Central Slave Mantle Conductor beneath the middle of the Slave Craton (Jones *et al.* 2001, 2003), the mantle conductor beneath the Sask Craton lying within the middle of the Trans-Hudson Orogen (Jones *et al.* 2005), and the C1 conductor in the middle of the Gawler Craton (Thiel & Heinson 2013). For the first two carbon in graphite form above the graphite-diamond stability field was appealed to, whereas for the latter grain boundary phases imposed through plume interaction are postulated. We hesitate to relate our anomaly UMC to the Iceland plume induced magmatic intrusion, but are intrigued by the spatial correlation of the C1 anomaly with reduced velocities (∼2 per cent reduction) and by the spatial correlation of our anomaly with reduced velocity. Far more data are required to substantiate or refute that interpretation.

Finally, we note that the dominant features we are reporting on were all found by our careful 2-D inversion and were substantiated through 3-D forward and inverse modelling. Their geometries are modified somewhat, but to second-order compared to their existence and location.

ACKNOWLEDGEMENTS

We thank Clare Horan, Gerry Wallace, Jessica Sprat, Marisa Adlem, Mark Hamilton, Anna Avdeeva and Louise Collins for helping in the field during collection of the data. We also thank local farmers for providing the farm land for MT site installations and logistic help on sites. It is our pleasure to acknowledge the help we received from Coillte officials for giving permission to install MT sites in different regions during 2005 field campaign. We also thank the Geological Survey of Canada for the loan of the LiMS systems, and the GIPP for lending the GEOMAGNET systems. UW thanks Gary Egbert for providing the ModEM software package for the presented

3-D inversion studies. CKR is thankful to S.K. Arora for helpful suggestions on the manuscript. Project funding from IRCSET Basic Research Grant SC/2003/237 to AGJ gratefully acknowledged.

We would like to thank the handling Editor, Gary Egbert, and the many reviewers of the four versions of this paper. Their comments served to require us to substantiate the conclusions in our original version, submitted in 2012 April, through exhaustive inversions and testing, but none of the subsequent 3-D inversions changed these conclusions in any major way.

REFERENCES

Al-Kindi, S., White, N., Sinha, M., England, R. & Tiley, R., 2003. Crustal trace of a hot convective sheet, *Geology,* **31,** 207–210.

Anderson, T.B. & Oliver, G.J.H., 1986. The Orlock Bridge Fault: a major late Caledonian sinistral fault in the Southern Uplands terrane, British Isles, Transactions of the Royal Society of Edinburgh, *Earth Sci.,* **77,** 203–222.

Anderson, F., Boerner, B.B., Harding, K., Jones, A.G., Kurtz, R.D., Parmelee, J & Trigg, D., 1988. LIMS: long period intelligent magnetotelluric system., *Presented at 9th Workshop on EM Induction in the Earth,* Sochi, USSR.

Archer, J.B., 1981. The Lower Palaeozoic rocks of the north western part of the Devilsbit-Keeper Hill inlier and their implications for the postulated course of the Iapetus suture in Ireland, *J. Earth Sci., R. Dublin Soc.,* **4,** 21–38.

Arrowsmith, S.J., Kendall, M., White, N., VanDecar, J.C. & Booth, D.C., 2005. Seismic imaging of a hot upwelling beneath the British Isles, *Geology,* **33,** 345–348.

Banks, R.J., Livelybrooks, D., Jones, P. & Longstaff, R., 1996. Causes of high crustal conductivity beneath the Iapetus suture zone in Great Britain, *Geophys. J. Int.,* **124,** 433–455.

Brock, A., 1989. Heat flow measurement in Ireland, *Tectonophysics,* **164,** 231–236.

Brown, C. & Whelan, J.P., 1995. Terrane boundaries in Ireland inferred from the Irish magnetotelluric profile and other geophysical data, *J. geol. Soc. Lond.,* **152,** 523–534.

Brown, C., Denny, P., Haak, V. & Bruton, P. the VARNET Group, 2003. VARNET MT: interpretation of magnetotelluric data over the Killarney-Mallow fault zone in south-west Ireland, *Irish J. Earth Sci.,* **21,** 1–17.

Chadwick, R.A. & Pharaoh, T.C., 1998. The seismic reflection Moho beneath the United Kingdom and adjacent areas, *Tectonophysics,* **299,** 255–279.

Chave, A.D. & Thompson, D.J., 2004. Bounded influence magnetotelluric response function estimation, *Geophys. J. Int.,* **157,** 988–1006.

Cliff, P.D., Carter, A. & Hurford, A.J., 1998. The erosional and uplift history of NE Atlantic passive margins: constraints on passing plume, *J. geol. Soc. Lond.,* **155,** 787–800.

Daly, J.S., 2001. The Precambrian, in *Geology of Ireland,* 2nd edn, pp. 7–45, ed Holland, C.H., Scottish Academic Press.

deGroot-Hedlin, C., 1991. Removal of static shift in two dimensions by regularized inversion, *Geophysics,* **56,** 2102–2106.

Denny, P., 2000. *A magnetotelluric and magnetovariational analysis of Variscan–Caledonian Southwest Ireland, PhD thesis,* National University of Ireland, Galway.

Dewey, J.F., 1969. Evolution of the Caledonian/Appalachian orogen, *Nature,* **222,** 124–129.

Dewey, J.F., 1988. Lithospheric stress, deformation and tectonic cycles: the disruption of Pangaea and the closure of Tethys, in Gondwana and Tethys, *Geol. Soc. London, Special Publication,* eds Audley-Charles, M.G. & Hallam, A, **37,** 23–40.

Do, V.C., Readman, P.W., O'Reilly, B.M. & Landes, M., 2006. Shear-wave splitting observations across southwest Ireland, *Geophy. Res. Lett.,* **33,** L03309, doi:10.1029/2005GL024496.

Duba, A.G. & Shankland, T.J., 1987. Analyzing electromagnetic data: suggestions from laboratory measurements, *Pure appl. Geophys.,* **125**(2–3), 285–290.

Duba, A.G., Heikamp, S., Meurer, W., Nover, G. & Will, G., 1994. Evidence from borehole samples for the role of accessory minerals in lower crustal conductivity, *Nature,* **367,** 59–61.

Edwards, R.N., Law, L.K. & White, A., 1971. Geomagnetic variations in the British Isles and their relation to electrical currents in the ocean and shallow seas, *Phil. Trans. R. Soc. Lond.,* **270**(1204), 289–323.

Egbert, G.D. & Kelbert, A., 2012. Computational recipes for electromagnetic inverse problems, *Geophys. J. Int.,* **189,** 251–267.

Evans, R.L. *et al.*, 2011. The electrical lithosphere beneath the Kaapvaal Craton, Southern Africa., *J. geophys. Res.,* **116,** B04105, doi: 10.1029/2010JB007883.

Frost, B.R., Fyfe, W.S., Tazki, K. & Chan, T., 1989. Grain-boundary graphite in rocks and implications of high electrical conductivity in the lower crust, *Nature,* **340,** 134–136.

Fullea, J., Muller, M.R., Jones, A.G. & Afonso, J.C., 2014. The lithosphere-asthenosphere system beneath Ireland from integrated geophysical-petrological modelling II: 3-D thermal and compositional structure, *Lithos,* **189**, 49–64.

Hansen, P.C., 1992. Analysis of discrete ill-posed problems by means of the L-curve, *Siam Rev.,* **34,** 561–580.

Harinarayana, T., Hutton, V.R.S. & Jones, P.C., 1993. Lateral variations of conductivity structure across southern Scotland and northern England, *Phys. Earth planet. Inter.,* **81,** 25–41.

Hauser, F., O'Reilly, B.M., Readman, P.W., Daly, J.S. & Van den Berg, R., 2008. Constraints on crustal structure and composition within a continental suture zone in the Irish Caledonides from shear wave wide-angle reflection data and lower crustal xenoliths, *Geophys. J. Int.,* **175**(3), 1254–1272.

Hejlet, S.-E. & Korja, T., 1993. Lithospheric and upper-mantle structures, results of electromagnetic soundings in Europe, *Phy. Earth planet. Inter.,* **79,** 137–177.

Hodgson, J., 2001. A seismic and gravity study of the Leinster Granite: SE Ireland, *PhD thesis,* Dublin Institute for Advanced Studies, Ireland.

Hutton, V.R.S. & Jones, A.G., 1980. Magnetovariational and magnetotelluric investigations in S. Scotland., in *Electromagnetic Induction in the Earth and Moon*, pp. 141–150, ed. Schmucker, U. & Arculus, AEPS-9, Centr. Acad. Publ. Japan, Tokio and D. Reidel Publ. Co., Dordrecht, Suppl. Issue J. Geomagn. Geoelectr.

Hutton, V.R.S., Sik, J.M. & Gough, D.I., 1977. Electrical conductivity and tectonics of Scotland, *Nature,* **266,** 617–620.

Jacob, A.W.B., Kaminski, W., Murphy, T., Phillips, W.E.A. & Prodehl, C., 1985. A crustal model for a northeast-southwest profile through Ireland, *Tectonophysics,* **113,** 75–103.

Jain, S., 1964. Electrical conductivity of the crust and upper mantle at Eskdalemuir, southern Scotland, *Nature,* **203,** 631–632.

Jones, A.G., 1983. The problem of "current channelling": a critical review. *Geophys. Surv. (Now Surv. Geophys.),* **6,** 79–122.

Jones, A.G., 1988. Static of magnetotelluric data and its removal in sedimentary basin environment, *Geophysics,* **53,** 967–978.

Jones, A.G., 1992. Electrical conductivity of the continental lower crust, in *Continental Lower Crust,* Chap. **3**, pp. 81–143, eds Fountain, D.M., Arculus, R.J. & Kay, R.W., Elsevier Publishers.

Jones, A.G., 1999. Imaging the continental upper mantle using electromagnetic methods, *Lithos,* **48,** 57–80.

Jones, A.G., 2011. Three-dimensional galvanic distortion of three-dimensional regional conductivity structures: comments on "Three-dimensional joint inversion for magnetotelluric resistivity and static shift distributions in complex media" by Y. Sasaki and M.A. Meju, 2006. *J. geophys. Res*., **116,** B12104, doi: 10.1029/2011JB008665.

Jones, A.G., 2012. Distortion of magnetotelluric data: its identification and removal. in *The Magnetotelluric Method: Theory and Practice*, pp. 219–302, eds Chave, A.D. & Jones, A.G. Cambridge Univ. Press.

Jones, A.G. & Hutton, V.R.S., 1977. Magnetotelluric investigation of the Eskdalemuir anomaly in S. Scotland, *Acta Geodaetica, Geophysica et Montanistica,* **12,** 111–115.

Jones, A.G. & Hutton, V.R.S., 1979a. A multi-station magnetotelluric study in southern Scotland 1. Field work, data analysis and results, *Geophys. J. R. astr. Soc.,* **56,** 329–349.

Jones, A.G. & Hutton, V.R.S., 1979b. A multi-station magnetotelluric study in southern Scotland 2. Monte-Carlo inversion of the data and its geophysical and tectonic implications, *Geophys. J. R. astr. Soc.,* **56,** 351–368.

Jones, A.G. & Jödicke, H., 1984. Magnetotelluric transfer function estimation improvement by coherent based technique, in *Proceedings of the 54th Annual International Meeting of Soc. Expl. Geophysics,* Atlanta, GA, Dec. 2–6.

Jones, A.G., Chave, A.D., Alud, D., Bahr, K. & Egbert, G., 1989. A comparison of techniques for magnetotelluric response function estimation, *J. geophys. Res.,* **94,** 14201–14213.

Jones, A.G., Ferguson, I.J., Chave, A.D., Evans, R.L. & McNeice, G.W., 2001. Electric lithosphere of the Slave craton, *Geology,* **29,** 423–426.

Jones, A.G., Lezaeta, P., Ferguson, I.J., Chave, A.D., Evans, R.L., Garcia, X. & Spratt, J., 2003. The electrical structure of the Slave craton, *Lithos,* **71,** 505–527.

Jones, A.G., Ledo, J. & Ferguson, I.J., 2005. Electromagnetic images of the Trans-Hudson Orogen: the North American Central Plains anomaly revealed, *Can. J. Earth Sci.,* **42,** 457–478.

Jones, A.G., Fullea, J., Evans, R.L. & Muller, M.R., 2012. Water in cratonic lithosphere: Calibrating laboratory-determined models of electrical conductivity of mantle minerals using geophysical and petrological observations, *Geochem. Geophys. Geosyst.,* **13,** Q06010, doi: 10.1029/2012gc004055.

Jones, A.G., Afonso, J.C., Fullea, J. & Salajegheh, F., 2014. The lithosphere-asthenosphere system beneath Ireland from integrated geophysical-petrological modelling – I: observations, 1D and 2-D hypothesis testing and modeling, *Lithos,* **189**, 28–48.

Karato, S., 1990. The role of hydrogen in the electrical conductivity of the upper mantle, *Nature,* **347,** 272–273.

Klemme, H.D. & Ulmishek, G.F., 1991. Effective petroleum source rocks of the world: stratigraphic distribution and controlling depositional factors, *AAPG Bull.,* **75,** 1809–1851.

Klemperer, S.L., Ryan, P.D. & Snyder, D.B., 1991. A deep seismic reflection transect across the Irish Caledonides, *J. geol. Soc. Lond.,* **148,** 149–164.

Korja, T., Smirnov, M., Pederson, L.B. & Gharibi, M., 2008. Structure of the central Scandinavian Caledonides and the underlying Precambrian basement, new constraints from magnetotellurics, *Geophys. J. Int.,* **175,** 55–69.

Landes, M., Prodehl, C., Hauser, F., Jacob, A.W.B. & Vermeulen, N.J., 2000. VARNET-96: influence of Variscan and Caledonian orogenies on crustal structure in SW Ireland, *Geophys. J. Int.,* **140,** 660–676.

Landes, M., O'Reilly, B.M., Readman, P.W., Shannon, P.M. & Prodehl, C., 2003. VARNET-96: 3-D upper-crustal velocity structure of SW Ireland, *Geophys. J. Int.,* **153,** 424–442.

Landes, M., Ritter, J.R.R., Do, V.C., Readman, P.W. & O'Reilly, B.M., 2004. Passive teleseismic experiment explores the deep subsurface of southern Ireland, *EOS, Trans. Am. geophys. Un.,* **85,** 337–341.

Landes, M., Ritter, J.R.R., Readman, P.W. & O'Reilly, B.M., 2005. A review of the Irish crustal structure and signatures from the Caledonian and Variscan Orogenies, *Terra Nova,* **17**(2), 111–120.

Landes, M., Ritter, J.R.R., O'Reilly, B.M., Readman, P.W. & Do, V.C., 2006. A N-S receiver function profile across the Variscides and Caledonides in SW Ireland, *Geophys. J. Int.,* **166,** 814–824.

Landes, M., Ritter, J.R.R. & Readman, P.W., 2007. Proto-Iceland plume caused thinning of Irish lithosphere, *Earth, planet. Sci. Lett.,* **255,** 32–40.

Ledo, J., 2005. 2-D versus 3-D magnetotelluric data interpretation, *Surv. Geophys.,* **26,** 511–543.

Ledo, J., Queralt, P., Marti, A. & Jones, A.G., 2002. Two-dimensional interpretation of three-dimensional magnetotelluric data: an example of limitations and resolution, *Geophys. J. Int.,* **150,** 127–139.

Leggett, J.K., 1978. Eustacy and pelagic regimes in the Iapetus Ocean during the Ordovician and Silurian, *Earth planet. Sc. Lett.,* **41,** 163–169.

Livelybrooks, D., Banks, R.J., Parr, R.S. & Hutton, V.R.S., 1993. Inversion of electromagnetic induction data for the Iapetus suture zone in the UK, *Phys. Earth planet. Inter.,* **81,** 67–84.

Long, Bary 2003. Ireland's vanished Ocean, *Earth Sci. 200, ES2K Newsletter,* **7,** 7–9.

Lowe, C. & Jacob, A.W.B., 1989. A north-south seismic profile across the Caledonian suture zone in Ireland, *Tectonophysics,* **168,** 297–318.

McKay, A.J. & Whaler, K.A., 2006. The electric field in northern England and southern Scotland: implications for geomagnetically induced currents, *Geophys. J. Int.,* **167,** 613–625.

McKerrow, W. & Cocks, L., 1986. Oceans, island arcs and olistostromes: the use of fossils in distinguishing structures, terranes and environments around the Iapetus Ocean, *J. geol. Soc. Lond.,* **143,** 185–191.

McNiece, G. & Jones, A.G., 2001. Multisite, multifrequency tensor decomposition of magnetotelluric data, *Geophysics,* **66,** 158–173.

Mackie, R.L. & Booker, J.R., 1999. *Documentation for mtd3fwd and d3-to-mt,* GSY-USA, Inc., San Francisco, CA.

Matte, P., 1986. Tectonics and plate tectonics model for the Variscan belt of Europe, *Tectonophysics,* **126,** 329–374.

Max, M.D., Ryan, P.D. & Inamdar, D.D., 1983. A magnetic deep structural geology interpretation of Ireland, *Tectonics,* **2,** 431–452.

Meqbel, N., 2009. The electrical conductivity structure of the Dead Sea Basin derived from 2-D and 3-D inversion of magnetotelluric data, *PhD thesis*, FU Berlin, Germany, Available at: http://www.diss.fu-berlin.de/diss/receive/FUDISS_thesis_000000014185?lang=en.

Moorkamp, M., Jones, A.G. & Eaton, D.W., 2007. Joint inversion of teleseismic receiver functions and magnetotelluric data using a genetic algorithm: Are seismic velocities and electrical conductivities compatible? *Geophys. Res. Lett.,* **34,** L16311, doi:10.1029/2007GL030519.

Moorkamp, M., Jones, A.G. & Fishwick, S., 2010. Joint inversion of receiver functions, surface wave dispersion and magnetotelluric data, *J. geophys. Res.,* **115,** B04318, doi:10.1029/2009JB006369.

Murphy, F.C., Anderson, T.B. & Daly, J.S., 1991. An appraisal of Caledonian suspect terrains in Ireland, *Irish J. Earth Sci.,* **11,** 11–41.

Narod, B.B. & Bennest, J.R., 1990. Ring-core fluxgate magnetometers for use as observatory variometers, *Phys. Earth plant. Inter.,* **59,** 23–28.

O'Donnell, J.P., Daly, E., Tiberi, C., Bastow, I.D., O'Reilly, B.M., Readman, P.W. & Hauser, F., 2011. Lithosphere-asthenosphere interaction beneath Ireland from joint inversion of teleseismic P-wave delay times and GRACE gravity, *Geophys. J. Int.,* **184,** 1379–1396.

Ogawa, Y., Jones, A.G., Unsworth, M.J., Booker, J.R., Lu, X., Craven, J., Roberts, B., Parmelee, J. & Farquharson, C., 1996. Deep electrical conductivity structures of the Appalachian orogen in the southeastern U.S., *Geophys. Res. Lett.,* **23,** 1597–1600.

O'Reilly, B.M., Readman, P.W. & Murphy, T., 1996. The gravity signature of Caledonian and Variscan tectonics in Ireland, *Phys. Chem. Earth,* **21,** 299–304.

Parr, R.S. & Hutton, V.R.S., 1993. Magnetotelluric studies in adjacent to the Northumberland basin, northern England, *Phy. Earth planet. Inter.,* **81,** 43–66.

Philcox, M., Savastopulo, G.D. & MacDermot, C.V., 1989. Intra-Dinantian tectonic activity on the Curlew Fault, north-west Ireland, the role of tectonics in Devonian and Carboniferous sedimentation in British Isles, *Yorkshire Geol. Soc.,* **6,** 55–66.

Phillips, W.E.A., Stillman, C.J. & Murphy, T., 1976. A Caledonian plate tectonic model, *J. geol. Soc. Lond.,* **132,** 579–609.

Polat, G., Lebedev, S., Readman, P.W., O'Reilly, B.M. & Hauser, F., 2012. Anisotropic Rayleigh-wave tomography of Ireland's crust: implications for crustal accretion and evolution within the Caledonian Orogen, *Gephys. Res. Lett*., **38**(5), L05304, doi:10.1029/2010GL046358.

Pous, J., Munoz, G., Heise, W., Melgarejo, J.C. & Quesada, C., 2004. Electromagnetic imaging of Variscan crustal structures in SW Iberia: the role of interconnected graphite, *Earth planet. Sci. Lett.,* **217,** 435–450.

Preston, J., 2009. Tertiary igneous activity, in *The Geology of Ireland,* pp. 333–354, eds Holland, C.H. & Sanders, I.S., Dunedin Academic Press.

Rao, C.K., Jones, A.G. & Moorkamp, M., 2007. The geometry of the Iapetus suture zone in central Ireland deduced from a magnetotelluric study, *Phys. Earth planet. Inter.,* **161,** 134–141.

Rousseeuw, P.J., 1984. Least median of squares regression, *J. Am. Stat. Assoc.,* **79,** 871–880.

Rousseeuw, P.J. & Leroy, A.M., 1987. *Robust Regression and Outlier Detection,* Wiley, pp. 335.

Ryan, P.D. & Devy, J.F., 1991. A geological and tectonic cross-section of the Caledonides of western Ireland, *J. geol. Soc. Lond.,* **148,** 173–180.

Ryan, P.D., Stillman, C.J., Allen, M. & Pow, S., 1995. Terrane geochemistry contrasts across the Iapetus Suture in Ireland, *Geol. Mag.,* **132**(5), 581–597.

Readman, P.W., O'Reilly, B.M. & Murphy, T., 1997. Gravity gradients and upper-crustal tectonic fabrics, Ireland, *J. geol. Soc. Lond.,* **154,** 817–828.

Ritter, O., Junge, A. & Dawes, G.J., 1998. New equipment and processing for magnetotelluric reference observation, *Geophys. J. Int.,* **132,** 535–548.

Rodi, W. & Mackie, R.L., 2001. Nonlinear conjugate gradients algorithm for 2-D magnetotelluric inversion, *Geophysics,* **66,** 174–187.

Roux, E., Moorkamp, M., Jones, A.G., Bischoff, M., Endrun, B., Lebedev, S. & Meier, T., 2011. Joint inversion of long-period magnetotelluric data and surface-wave dispersion curves for anisotropic structure: Application to data from Central Germany. *Geophys. Res. Lett.,* **38**(5), L05304, doi:10.1029/2010GL046358.

Shankland, T.J. & Waff, H.S., 1997. Partial melting and electrical conductivity anomalies in the upper mantle, *J. geophys. Res.,* **82,** 5409–5417.

Sevastopulo, G.D., 1982. The age and depositional setting of Waulsortain limestones in Ireland, in *Proceedings of Symposium on Palaeoenvironmental Setting and Distribution of Waulsortian Facies*, pp. 65–79, eds Bolton, K., Lane, R.H. & Le Monde, D.V., El Paso Geol. Soc. and the University of Texas at El Paso.

Siripunvaraporn, W., Egbert, G., Lenbury, Y. & Uyeshima, M., 2005. Three-dimensional magnetotelluric inversion: data-space method, *Phys. Earth planet. Inter.,* **150**(1–3), 3–14.

Soper, N.J., Ryan, P.D. & Dewey, J.F., 1999. Age of the Grampian orogeny in Scotland and Ireland, *J. geol. Soc. Lond.,* **156,** 1231–1236.

Sule, P.O. & Hutton, V.R.S., 1986. A broad-band magnetotelluric study in southeastern Scotland - Data acquisition, analysis and one-dimensional modeling, *Ann. Geophys. Ser. B-Terrest. Planet. Phys.,* **4,** 145–155.

Sule, P.O., Hutton, V.R.S. & Dumitrescu, C., 1993. Subsurface structure of SE Scotland from broad-band magnetotelluric measurements, *Phy. Earth planet. Inter.,* **81,** 91–24.

Tauber, S., Banks, R., Ritter, O., Weckmann, U. & Junge, A., 2003. A high-resolution magnetotelluric survey of the Iapetus suture zone in southwest Scotland, *Geophys. J. Int.,* **153,** 548–568.

Thiel, S. & Heinson, G., 2013. Electrical conductors in Archean mantle - Result of plume interaction?, *Geophys. Res. Lett.,* **40,** 2947–2952.

Tietze, K. & Ritter, O., 2013. Three-dimensional magnetotelluric inversion in practice-the electrical conductivity structure of the San Andreas Fault in Central California, *Geophys. J. Int.,* **195,** 130–147.

Todd, S.P., Murphy, F.C. & Kennan, P.S., 1991. On the trace of Iapetus suture in Ireland and Britain, *J. geol. Soc. Lond.,* **148,** 869–880.

Trabucho-Alexandre, J., Hay, W.W. & De Boer, P.L., 2012. Phanerozoic environments of black shale deposition and the Wilson Cycle, *Solid Earth,* **3,** 29–32.

Van den Berg, R., Stephan Daly, J. & Salisbury, M.H., 2005. Seismic velocities of granulite-facies xenoliths from central Ireland: implications for lower crustal composition and anisotropy, *Tectonophysics,* **407,** 81–99.

Wannamaker, P. E., Hohmann, G.W. & Ward, S. H., 1984. Magnetotelluric responses of 3-dimensional bodies in layered Earths, *Geophys,* **49,** 1517–1533.

Wannamaker, P.E. *et al.*, 1996. Magnetotelluric experiment probes deep physical state of southeastern U.S., *EOS, Trans. Am. geophys. Un., 77*(34), 329–333.

Wawerzinek, B., Ritter, J.R.R., Jordan, M. & Landes, M., 2008. An upper-mantle upwelling underneath Ireland revealed from non-linear tomography, *Geophys. J. Int.,* **175**(1), 253–268.

Weckmann, U., 2012. Making and breaking of a continent: following the scent of geodynamic imprints on the African continent using electromagnetics, *Surv. Geophys.,* **33,** 107–134.

Weckmann, U., Magunia, A. & Ritter, O., 2005. Effective noise separation for magnetotelluric single site data processing using a frequency domain selection scheme, *Geophys. J. Int.,* **161**(3), 635–653.

Whelan, J.P., Brown, C., Hutton, V.R.S. & Dawes, G.K.K., 1990. A geoelectric section across Ireland from magnetotelluric soundings, *Phys. Earth planet. Inter.,* **60,** 138–146.

Wilson, J.T., 1966. Did the Atlantic close and then re-open? *Nature,* **211,** 676–681.

Woodcock, N.H., Soper, N.J. & Strachan, R.A., 2007. A Rheic cause for the Acadian deformation in Europe, *J. geol. Soc. Lond.,* **164,** 1023–1036.